Kinetics of the reaction of the heaviest hydrogen atom with H_2, the $^4He\mu + H_2 \rightarrow {}^4He\mu H + H$ reaction: Experiments, accurate quantal calculations, and variational transition state theory, including kinetic isotope effects for a factor of 36.1 in isotopic mass

Donald G. Fleming,[1,a)] Donald J. Arseneau,[1] Oleksandr Sukhorukov,[1,b)] Jess H. Brewer,[2] Steven L. Mielke,[3] Donald G. Truhlar,[3,a)] George C. Schatz,[4] Bruce C. Garrett,[5] and Kirk A. Peterson[6]

[1]*TRIUMF and Department of Chemistry, University of British Columbia, Vancouver, British Columbia V6T 1Z1, Canada*
[2]*Department of Physics, University of British Columbia, Vancouver, British Columbia V6T 1Z1, Canada*
[3]*Department of Chemistry and Supercomputing Institute, University of Minnesota, Minneapolis, Minnesota 55455-0431, USA*
[4]*Department of Chemistry, Northwestern University, Evanston, Illinois 60208-3113, USA*
[5]*Chemical and Material Sciences Division, Pacific Northwest National Laboratory, Richland, Washington 99352, USA*
[6]*Department of Chemistry, Washington State University, Pullman, Washington 99164-4630, USA*

(Received 23 August 2011; accepted 10 October 2011; published online 14 November 2011)

The neutral muonic helium atom $^4He\mu$, in which one of the electrons of He is replaced by a negative muon, may be effectively regarded as the heaviest isotope of the hydrogen atom, with a mass of 4.115 amu. We report details of the first muon spin rotation (μSR) measurements of the chemical reaction rate constant of $^4He\mu$ with molecular hydrogen, $^4He\mu + H_2 \rightarrow {}^4He\mu H + H$, at temperatures of 295.5, 405, and 500 K, as well as a μSR measurement of the hyperfine coupling constant of muonic He at high pressures. The experimental rate constants, $k_{He\mu}$, are compared with the predictions of accurate quantum mechanical (QM) dynamics calculations carried out on a well converged Born–Huang (BH) potential energy surface, based on complete configuration interaction calculations and including a Born–Oppenheimer diagonal correction. At the two highest measured temperatures the agreement between the quantum theory and experiment is good to excellent, well within experimental uncertainties that include an estimate of possible systematic error, but at 295.5 K the quantum calculations for $k_{He\mu}$ are below the experimental value by 2.1 times the experimental uncertainty estimates. Possible reasons for this discrepancy are discussed. Variational transition state theory calculations with multidimensional tunneling have also been carried out for $k_{He\mu}$ on the BH surface, and they agree with the accurate QM rate constants to within 30% over a wider temperature range of 200–1000 K. Comparisons between theory and experiment are also presented for the rate constants for both the $D + H_2$ and $Mu + H_2$ reactions in a novel study of kinetic isotope effects for the $H + H_2$ reactions over a factor of 36.1 in isotopic mass of the atomic reactant. © *2011 American Institute of Physics*. [doi:10.1063/1.3657440]

I. INTRODUCTION

Isotopic substitution has long been a valuable tool for mechanistic analysis and testing of fundamental theories of chemical kinetics. In the Born–Oppenheimer (BO) approximation, the potential energy surface (PES) is independent of the nuclear masses, and this simplifies the calculation of kinetic isotope effects (KIEs), which are the ratios of rate constants for two reactions differing only in isotopic masses. Although KIEs can be measured for any isotopic substitutions, exemplified by the substitution of ^{13}C for ^{12}C (mass ratio of 1.08), the largest KIEs are found at the lowest end of the mass scale, and they are historically associated with the substitution of D (deuterium) for ^1H. Although the use of T (tritium) allows for KIEs with a mass ratio of 3, thermal reaction rate studies of T atom kinetics have rarely been carried out, in part because tritium is difficult to handle, being dangerously radioactive. Thus it has fallen to muon science to extend the H-atom isotopic mass scale in reaction rate studies beyond its normally accessible range.[1,2]

The *lightest* H atom isotope is muonium ($Mu \equiv \mu^+e^-$), formed by charge exchange when a positive muon (μ^+) takes an electron from surrounding material to form the neutral Mu atom.[3,4] Although lacking a nucleus in the conventional (hadronic) sense, the muon is still ~207 times heavier than an electron, so Mu (unlike positronium) behaves chemically like a very light H atom, with a mass of only 0.114 amu. Due to its remarkably low mass, Mu has proved to be an unusually sensitive probe of quantum effects on nuclear motion in reaction rates, both in terms of zero-point-energy (ZPE) shifts and in

a)Authors to whom correspondence should be addressed. Electronic addresses: flem@triumf.ca and truhlar@umn.edu.
b)Present address: Department of Chemistry, University of Alberta, Alberta, Canada.

its propensity to manifest quantum tunneling.[5–22] In comparison with the reaction rates of ^{1}H, D, and T, the study of Mu reactivity allows comparisons between theory and experiment for isotopic mass ratios up to 27.

At the end of its slowing-down processes, a negative muon (μ^-), in contrast to a μ^+, is captured by an atom into a "muonic orbit,"[23,24] and, in the case of capture by atomic ^{4}He, forms the neutral ^{4}Heμ atom after charge-exchange with an added dopant (see below),[25,26] in which a μ^- has replaced one e^- in ^{4}He. With an atomic mass of 4.115 amu, the neutral muonic He atom (hereafter denoted Heμ) extends the isotopic mass scale in the opposite direction compared to Mu, giving effectively the *heaviest* isotope of the H-atom. The Heμ atom behaves as an isotope of hydrogen because the heavy mass of the negative muon leads to a muonic 1*s* orbital that is so close to the nucleus (a factor of ∼400 times closer than the electron 1*s* orbital) that the μ^- fully screens one proton charge. (The radionuclides ^{4}H, ^{5}H, ^{6}H, and ^{7}H have been reported but these are all unstable to neutron emission, and thus have very short lifetimes, $\sim 10^{-22}$ s,[27] making them experimentally inaccessible for reaction rate studies.) Past comparisons of the Lamb shift and the hyperfine coupling constant of muonic helium[25,28,29] with those of hydrogen and muonium[30] have drawn intense interest over the years because they provide important tests of quantum electrodynamics. However, the utility of muonic helium as an isotope of hydrogen in chemical reaction rates has, until recently,[31,32] gone largely unrealized.

In this paper, we report on the background to and experimental details for the kinetics study of this heaviest accessible isotope of the hydrogen atom, and in particular its reaction with molecular hydrogen, the Heμ + H_2 → HeμH + H reaction. Study of the H + H_2 reaction has long played a key role in extending our understanding of reaction dynamics,[33–36] and herein we exploit the unparalleled accuracy of theory for this system, both in terms of the PES and the quantum dynamical calculations, to compare with these Heμ + H_2 results. Experimental rate constants were determined at 295.5, 405, and 500 K and were briefly reported on earlier;[32] these results completely supersede some preliminary data at 295.5 K reported in a conference proceedings.[31] The experimental data are compared with theoretical results from accurate quantum mechanical (QM) calculations and variational transition state theory (VTST) methods. The results here are also compared with analogous studies for the Mu + H_2 reaction reported in 1987 (Ref. 9) and with results for D + H_2,[37–42] with a view to providing a novel study of KIEs over a range of a factor of 36.1 in isotopic mass.

II. FORMATION OF Heμ AND MEASUREMENT OF ITS HYPERFINE COUPLING CONSTANT BY μSR

Due to the nuclear weak interaction, muon beams (μ^+ and μ^-) can be produced from pion ($\pi^+$and π^-) decay with almost 100% longitudinal spin polarization[4,24] at an accelerator such as TRIUMF, where the present experiments were carried out. In the subsequent decay of a muon ($\mu^\pm \rightarrow e^\pm \nu\bar{\nu}$), the resulting $e^\pm$, which is detected in the experiments, is emitted preferentially *along* the muon spin direction in the case of μ^+ decay, or in the *opposite direction* for μ^- decay. The latter

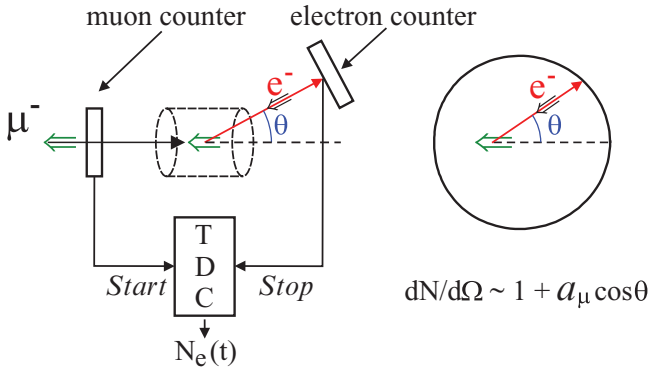

FIG. 1. Schematic of the experimental apparatus (left) and the anisotropy pattern of decay electrons (right). The incident negative muon (μ^-), which is polarized opposite (green arrow) to its momentum direction (black arrow), triggers a "muon counter" and starts a time-to-digital converter (TDC), which is stopped by the detection of a decay electron in an "electron counter" positioned at a fixed angle, θ, with respect to the incident muon beam. In this experiment the energy-averaged "asymmetry'', a_μ, is measured and has a nominal value of $a_\mu = 1/3$, and this is the decay pattern shown on the right.

case, of principal interest here, is shown schematically, along with a simple counter arrangement, in Fig. 1. The incident polarized μ^- (green arrow) triggers a counter, sending a "start'' signal to a time-to-digital converter (TDC), before stopping in the target; it later decays ($\tau = 2.197$ μs for a bare muon), emitting its decay e^- (with the same helicity as the incident μ^-), which triggers a second counter, sending a "stop" signal to the TDC. In practice there are often 2–3 detectors in a "counter telescope" with various coincidences demanded as well as additional telescopes depending on the experimental environment.[26] The number of electrons detected within a time interval δt at time "t" between start and stop, $N(t)\delta t$, plotted vs. t, gives an experimental histogram of detected events. The anisotropy in the muon decay pattern mentioned above is shown on the right of Fig. 1, representative of an "asymmetry" of $a_\mu = 1/3$, appropriate for fully polarized μ^- after averaging over e^- decay energies. In a μSR (muon spin "relaxation" or "resonance" as well as "rotation") experiment, this anisotropy pattern will shift the counts away from exponential decays in each histogram bin depending on the angle (θ) between the muon spin direction and the electron counter at the time of decay (the time t of the bin). When the muon spin precesses in a magnetic field, this effect is seen as an oscillating signal on top of the exponential decay(s). In general, the muon polarization is distributed among several different environments initially, and is lost over time as well as precessing, such that the total asymmetry is $A(t) = \sum_i a_i(t)$. This is the basis of the μSR technique[3,4,26,43–46] employed here.

Although the kinetic energies of muon beams can be several MeV upon entering the gas target, most of this energy is lost to ionization and inelastic scattering processes down to energies of ∼100 keV.[3,4] In this "Bethe–Bloch" regime, which is essentially the same for μ^+ and μ^- beams, there is no loss in muon polarization because the muon spin is unaffected by what are basically Coulomb interaction processes. It is at lower energies that the fates of positive and negative muons differ. The μ^+ undergoes a series of charge-exchange (CE) cycles in a gas, emerging (in most gases) mainly as

muonium (Mu) with kinetic energies of ~10 eV, which then thermalizes to $\sim k_B T$ energies (where k_B is Boltzmann's constant and T is temperature) on a time scale of order 10 ns at densities equivalent to 1 bar at 300 K—much faster than typical (~ 1 μs) chemical reaction times for Mu with added reactants.[2–4,12,14,21] During this final thermalization process the muon polarization in Mu is shared with the electron, and, at observation times, may also be distributed among different environments including diamagnetic molecular products formed as a result of "hot" Mu reactions that occurred at epithermal energies.[1,2,4] At observation times, the μSR signal exhibits a high polarization in most molecular gases corresponding to an observed Mu fraction of typically about 80%.[4,44,47]

In marked contrast, μ^- particles at comparable energies of tens of keV are captured into high-l atomic orbitals and then rapidly cascade down to the muonic 1s state[23,26,45] in a time of ~0.1 ns for He.[26,29] The accompanying Auger processes usually eject both of the atomic electrons in He, leaving the positive $(\mathrm{He}\mu)^+$ ion, which, as with μ^+, can be neutralized in a CE collision with a dopant labeled X,

$$(\mathrm{He}\mu)^+ + X \rightarrow \mathrm{He}\mu + X^+, \qquad (1)$$

forming the neutral Heμ muonic atom (the name "muonic atom'' is used for the neutral species in this paper, although in the μ^- literature it also often denotes the positive ion that is formed by the cascade process[23,24]). These different capture and thermalization processes for μ^+ and μ^- beams are compared and contrasted in the schematic diagram shown in Fig. 2.

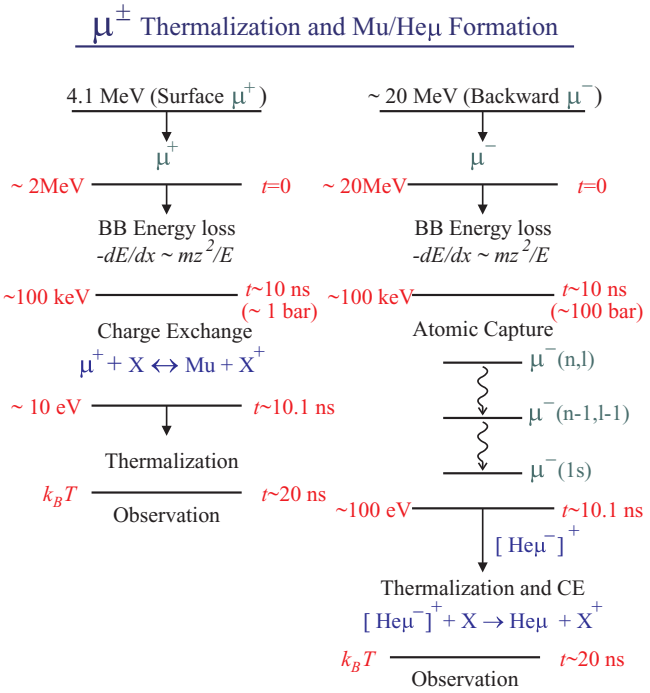

FIG. 2. Schematic of the energy/time domains for μ^+/μ^- thermalization and charge neutralization giving Mu/Heμ formation. For μ^+ (left), "surface μ^+ beams" are often used, from π^+ decay at rest [see Refs. 3, 4], where the incident energy is 4.1 MeV, which is reduced to ~2 MeV upon entering the gas target. For μ^- (right), this mode is not possible and thus "Backward μ^- beams" are used, from π^- decay in flight, in which the μ^- kinetic energy upon entering the gas target (see Fig. 1) is about 20 MeV, from the M9B channel at TRIUMF. In practice, backward μ^+ beams were also utilized in the present study. In both cases most of this incident energy is lost in the "Bethe–Bloch" regime, where the stopping power, $S(E)$ [see Ref. 3], is similar. At energies of ~100 keV, the μ^+ enters into a series of charge exchange cycles, emerging mainly as the neutral Mu atom. In the μ^- case, this process is atomic capture, emerging, in the case of helium, as the muonic He ion, $(\mathrm{He}\mu)^+$. This is then charge neutralized with a dopant (X) in a manner similar to Mu formation, but at or near thermal energies. It is the neutral Heμ atom that is the basis of the present study.

Unlike the case in Mu formation, the CE process in Eq. (1) is thought to proceed at near-thermal energies, so it is necessary to choose dopants with an ionization potential (IP) less than that of the neutral atom, which for Heμ is essentially the same as for other hydrogen isotopes, namely 13.6 eV. In almost all previous studies of Heμ formation, Xe (IP = 12.1 eV) has been used as the dopant but only very weak μSR signals with polarizations of ~1% were observed.[25,26,28] An exception is the work of Barton *et al.*,[29] where CH_4, though with a similar IP of 12.5 eV, was used as a dopant in an experiment with optically pumped Rb. This low polarization is partly due to preferential capture of the μ^- on the high $Z = 54$ Xe atom (the empirical Fermi–Teller Z law[23] predicts that the capture is proportional to Z) and partly due to additional depolarization mechanisms in the cascade process in He that are still not understood. (In the absence of other depolarization mechanisms, most $I = 0$ muonic atoms have residual μ^- polarizations in the 1s state of about 6%.[23,24,45])

In the present study NH_3 was used as the added dopant, also at the 1%–2% level (though at high total pressures) in the hope of seeing a larger signal, due both to its reduced total charge ($Z = 10$) and lower IP (10.8 eV). The latter could also be particularly important if complex molecular ions, $[(\mathrm{He}\mu)\mathrm{He}]^+$, with increased binding energy, were to form at the high He densities of the experiment. However, although some improvement was seen in the absence of added H_2 reactant,[31] the observed polarization was comparable to that reported earlier[26] in Xe and was reduced even further in the presence of large amounts of H_2 (at 295.5 K) due to μ^- capture on H_2 and hyperfine mixing[45] in the muonic H atom thus formed. Somewhat higher μ^- polarizations were seen at the higher temperatures (where the H_2 partial pressures are lower) but the values still remained rather low, necessitating long run times (~24 h) at all temperatures.

A Fourier transform (FT) of a precessing μSR signal will display peaks at characteristic frequencies, just as in NMR,[43] an example of which is shown in Fig. 3. The top spectrum shows the FT signals for a doping of 2.5% NH_3 in 290 bar He in a transverse magnetic field (TF) of 65.63 G. At this field there are two frequencies as shown, at 90.51 MHz and 94.30 MHz, which reflect the observable transitions of the hyperfine Hamiltonian in this field range for the Heμ atom.[26,28,48] These measured frequencies lead directly[26] to a determination of the hyperfine coupling constant (hfcc) between the μ^- and e^- spins, $\nu_0(\mathrm{He}\mu) = 4470 \pm 8$ MHz, determined in the present study from a weighted average of several μSR determinations at total pressures near 300 bar. This compares very well, and well within errors, with much more precise values determined earlier by an RF-resonance technique.[28,30] Gardner *et al.*[28] found only a small pressure shift on $\nu_0(\mathrm{He}\mu)$ and extrapolated from measurements at

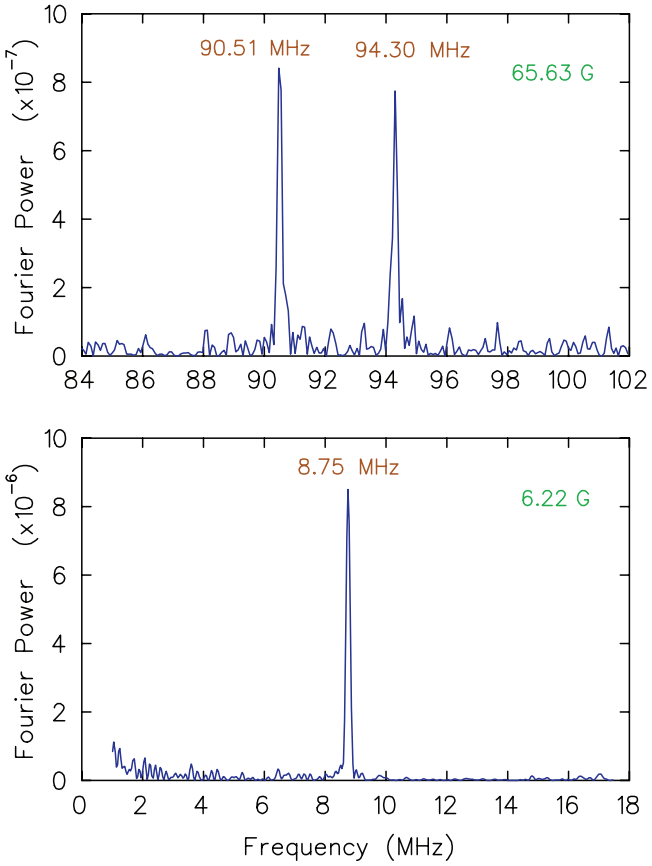

FIG. 3. In a transverse magnetic field (TF), the muon spin in the muonic He atom precesses at a characteristic frequency that depends on the field. Each time the muon spin sweeps past a fixed electron counter one detects its enhanced decay probability in the counter direction (Fig. 1), giving rise to an oscillatory pattern, which can be analyzed by Fourier transform (FT) spectroscopy. The figure shows the FT spectra for Heμ in the presence of about 7 bar NH_3 and He up to a total pressure of 300 bar. The upper spectrum shows two split frequencies determined in a transverse magnetic field of 65.63 G, from which the hyperfine coupling constant ν_0 can be determined.[26,31] The lower spectrum shows a single frequency at the low field of 6.22 G, where the energy splittings become degenerate. It is the observation of the time dependence of this signal (Figs. 4 and 5), and particularly its relaxation rate, upon which the experimental results are largely based.

pressures up to 18 bar to report a zero-pressure value of $\nu_0(\text{He}\mu) = 4465.005 \pm 0.029$ MHz. There is no indication from the present study of any additional pressure dependence. Despite the lesser precision, this result comes from the first observation of hyperfine splitting in the spin precession of Heμ. It was important to identify Heμ by its μSR signal while establishing that no other paramagnetic muonic spin states were present, and the measurement is also relevant to the claim below that this atom can indeed simply be treated as an isotope of hydrogen.

While confirmation of the observation of the muonic He atom at intermediate fields was important, the kinetics studies of interest were all carried out at much lower fields, where the splitting shown in Fig. 3 becomes negligible, and only a single frequency that corresponds to the classical limit of "triplet" Heμ precession is observed. This is shown in the bottom FT in Fig. 3, in a field of 6.22 G giving $\nu_{\text{He}\mu} = 8.75$ MHz, almost the same as would be shown by Mu precession in the same field.[31] The data analysis discussed below is based solely on this weak-TF μSR signal.

III. EXPERIMENTAL METHODS AND RESULTS

III.A. Target environment

The gas target for these experiments was a thick-walled 316 stainless steel vessel about 25 cm in length having a Ti (Ti6A14V) front flange with a muon entrance window 2.5 cm in diameter and 3 mm thick. It was heated by two Watlow cable heaters wound around the circumference in two locations that minimized internal temperature gradients. The entire vessel was placed inside a vacuum jacket for insulation and temperature stability. For runs at 295.5 K, the window and body temperature of the target cell were measured by thermocouples (TCs) placed on the cell exterior, but not controlled. At 405 and 500 K the gas temperature was measured and controlled by an additional TC placed inside the target vessel. The gas temperature was stable to within a degree over long run periods of 24 h or more. (Such long run periods actually helped to ensure T stability because fluctuations that invariably occur as a result of changing the gas load have ample time to re-equilibrate.) In addition, off-line measurements of a TC inserted at different positions along the length of the target vessel (at 1 atm) showed that the temperature gradient was less than 2 K over the extent of the muon stopping distribution, and could be expected to be even lower at the higher pressures of the experiments. The overall temperatures and uncertainties for each point have then been assessed as 295.5 ± 1.5, 405.0 ± 1.0, and 500.0 ± 1.5 K, and are referred to hereafter as 295.5, 405, and 500 K, respectively.

Relatively high H_2 concentrations were required in these experiments, particularly at 295.5 K, to ensure that the reaction rate for $\text{He}\mu + H_2 \rightarrow \text{He}\mu\text{H} + \text{H}$ would be fast enough to give a reliably measured Heμ spin relaxation rate constant, denoted $\lambda_{\text{He}\mu}$ below. This mandated high He pressures in order to minimize competitive μ^- capture on the H_2, which in turn dictated the use of "backward" μ^- beams ($\sim$70 MeV/c momentum or $\sim$20 MeV kinetic energy), as indicated in Fig. 2, in order to penetrate the thick Ti entrance window of the target vessel. Total pressures near 300 bar (from 290 to 335 bar) and 500 bar (from 495 to 510 bar) were run at 295.5 K in order to check for any effect of moderator pressure on the reaction rate, but at the higher temperatures only a pressure near 500 bar was employed. The small variations in pressure noted were due to different target fills and run periods and are not deemed significant. The majority constituent was He at all pressures with H_2 partial pressures varying up to 110 bar at 295.5 K, up to 11.5 bar at 405 K, and up to 2.5 bar at 500 K. The higher H_2 pressures (over 11.5 bar) were measured with one of two Bourdon-tube pressure gauges but lower values were measured with a Baratron capacitance manometer. The needle-gauge readings were only accurate to about $\pm$1.5 bar and $\pm$0.5 bar but the Baratron pressure readings were more accurate, with an uncertainty of $\sim$0.5% of the pressure. In addition, there were corrections for H_2 gas blown in from and diffusing into the transfer tube, taking into account the different temperatures between this tube and the target vessel. Total uncertainties for $[H_2]$ are shown in the plots to follow. These concentrations were calculated using a recent equation of state,[49] and were also in good agreement with long-established compressibility data.

The whole target assembly was placed in the center of the TRIUMF μSR Omni′ magnetic spectrometer positioned at the end of the backward-muon M9B beam line at TRIUMF. Two ~20 mm diameter collimators to define the incident muon beam were positioned just ahead of the target window. Transverse fields of about 6 G (for Heμ precession) and up to 100 G (for hyperfine coupling constant measurements) were applied vertically by Helmholtz coils. Decay electrons were detected by two (left/right) pairs of plastic scintillator counters in the plane of precession (recall Fig. 1). Incident gated μ^- intensity was about 50 000/s with about 1800 total good e^- decay events per second.

III.B. Data analysis and results

The experimental data are stored in time histograms generated by individual electron events: the time difference between the incident μ^- "start" and the detected e^- "stop" is recorded by a TDC, as indicated in Fig. 1, and the corresponding bin of the time histogram is incremented. After many millions of such events, the resulting time distribution is described by the function

$$N(t) = N_{\text{const}} + N_{\text{He}\mu} e^{-t/\tau_{\text{He}\mu}} \times [1 + A_{\text{He}\mu} e^{-\lambda_{\text{He}\mu} t} \cos(\omega_{\text{He}\mu} t + \varphi_{\text{He}\mu})] + \sum_i N_i e^{-t/\tau_i} [1 + A_i e^{-\lambda_{D,i} t} \cos(\omega_D t + \varphi_D)], \quad (2)$$

where N_{const} is a normalization term for time-independent background counts, $N_{\text{He}\mu}$ is a normalization for the signal from the neutral muonic helium atom, which contains the principal quantities of interest in these experiments (the neutral atom initial "asymmetry," $A_{\text{He}\mu}$, and its relaxation rate constant $\lambda_{\text{He}\mu}$), and the N_i are normalizations for different species formed by μ^- capture on different elements, each decaying with a different lifetime (τ_i) due to different nuclear capture rates.[31,46,50] One of these contributions is due to the $(\text{He}\mu)^+$ ion with $\tau_{\text{He}\mu^+} = 2.1953$ μs,[50] which is taken to be the same as the lifetime $\tau_{\text{He}\mu}$ of the neutral atom, and is close to the value for the positive muon, $\tau_{\mu^+} = 2.1970$ μs.[50]

The other parameters in Eq. (2) are $\omega_{\text{He}\mu}$, the Larmor precession frequency for the neutral muonic He atom, ω_D, the Larmor precession frequency for all diamagnetic environments, the relaxation rate constants $\lambda_{D,i}$ for those environments, and the corresponding initial phases ($\varphi_{\text{He}\mu}$or φ_D). In practice $\lambda_{D,i}$ was only determined for the muonic He component, because those for stops in the metal target window or walls of the target vessel had little or no diamagnetic contribution, as determined by measurements at higher magnetic fields, and no significant precession at ω_D in a 6 G field within the short μ^- lifetimes. Although a large number of elements could contribute to μ^- capture when considering the alloys of the reaction vessel, all possible contributions cannot be disentangled, and the number of terms was limited to four, including $(\text{He}\mu)^+$. A large background at the cyclotron's RF frequency (23 MHz), plus harmonics, likely originating from x-rays emitted by μ^- capture in the collimators, also had to be taken into account. This RF background was removed from the data prior to fitting it to Eq. (2) by subtracting the signal in $t < 0$ bins offset by multiples of the beam-pulse interval (43.3 ns).

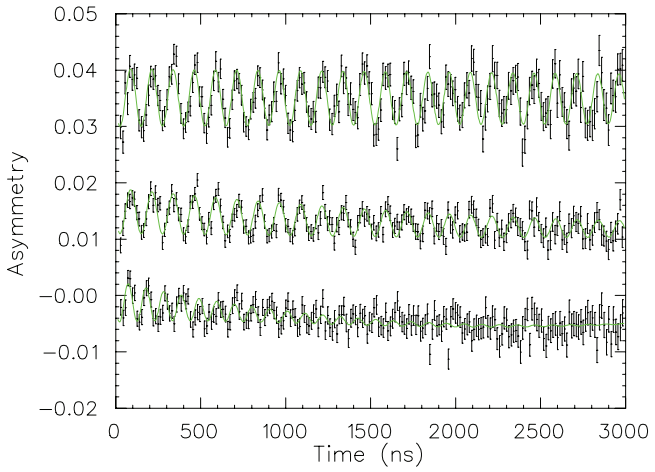

FIG. 4. Asymmetry plots for Heμ + H_2 at 295.5 K in a field of 6.8 G: (top) in a gas mixture of 7.2 bar NH_3 plus He to 300 bar; (middle) with 25 bar of added H_2 to give a concentration $[H_2] = 5.9\times10^{20}$ molecules cm^{-3}; (bottom) as in the top curve but with $[H_2] = 25.7\times10^{20}$ molecules cm^{-3} at 500 bar total pressure. The solid curves are fits of the "asymmetry" defined by Eq. (2). The observed signal is mainly characterized by the oscillations seen, due to the Larmor frequency $\omega_{\text{He}\mu}$, with initial amplitude $A_{\text{He}\mu}$ and relaxation rate constant, $\lambda_{\text{He}\mu}$. For $[H_2] = 0$ in the top plot, $\lambda_{\text{He}\mu}$ is just the background relaxation rate constant λ_b of Eq. (3), and is almost zero (see also Fig. 6). Note though in the middle and bottom plots that the relaxation rate increases and the amplitude decreases with increasing H_2 concentration.

Example data and fits are shown for different H_2 concentrations in Fig. 4 at 295.5 K and in Fig. 5 at 405 and 500 K, for gas mixtures with 7.2 bar NH_3 plus He to total pressures of ~300 bar or 500 bar in a field near 6 G (6.8 G and 5.7 G in different run periods). These plots have been transformed to show only the relaxing and precessing asymmetry signal. The solid green-line fits shown are dominated by the precession of the Heμ atom [the second term of Eq. (2)] with initial amplitude $A_{\text{He}\mu}$, since in such a low field the slow diamagnetic precession appears as a slight drift on the time scale displayed (particularly for the bottom curve in Fig. 4 with the highest $[H_2]$). In the case of $[H_2] = 0$ at 295.5 K (upper plot in Fig. 4), $A_{\text{He}\mu} = 0.005$ and there is essentially no relaxation, whereas in the next two plots $A_{\text{He}\mu}$ is decreasing with increasing $[H_2] = 5.9 \times 10^{20}$ and 25.7×10^{20} molecules cm^{-3}, respectively, due to competitive μ^- capture on the hydrogen; meanwhile, the relaxation rate, $\lambda_{\text{He}\mu}$ is increasing due to the Heμ + H_2 reaction. Though weak, with amplitudes $A_{\text{He}\mu}$ in the range ~0.003–0.005 from fits of Eq. (2) to the data, the μSR precession signals are nevertheless clearly visible at all temperatures. The maximum polarization here is only about 2%. (The polarization is the ratio of the observed amplitude to the value of $A_{\max}$, usually most reliably determined from stopping μ^+ beams in Ag metal, where there is no depolarization; in the present TRIUMF study, $A_{\max}$ is 0.29 ± 0.02 from a series of μ^+ runs in He and N_2 mixtures at total pressures from about 100 to 500 bar.) For reference, the corresponding observed amplitude for Mu precession is in the range ~0.04–0.07, an order of magnitude larger than $A_{\text{He}\mu}$.[31] It is noteworthy from Fig. 5, at much lower concentrations than in Fig. 4,

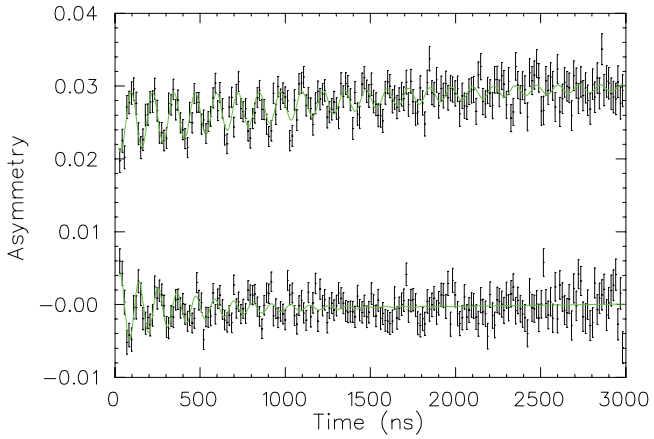

FIG. 5. Asymmetry plots for Heμ + H_2 in 7.2 bar NH_3 plus He to 500 bar in a 6.8 G TF, with $[H_2] = 0.87\times10^{20}$ molecules cm^{-3} at 405 K in the top plot, but with $[H_2] = 0.42\times10^{20}$ molecules cm^{-3} at 500 K in the bottom plot. See the caption to Fig. 4. The initial amplitudes $A_{He\mu}$ are both 0.005, close to maximum, but the relaxation rates $\lambda_{He\mu}$ are much faster at these temperatures, even at lower concentrations than in Fig. 4.

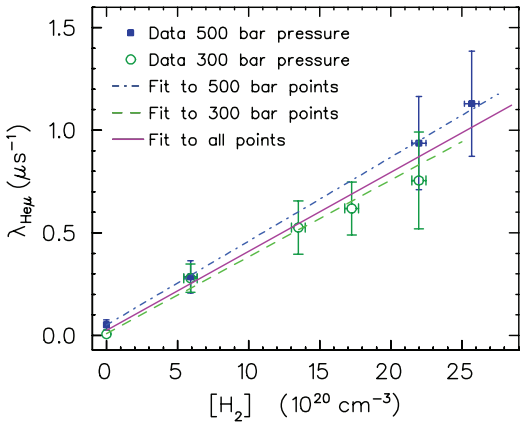

FIG. 6. Relaxation rate constants vs. $[H_2]$ from fits of Eq. (2) to the data for the Heμ + H_2 reaction at 295.5 K. The data were measured at two different total (mainly He) pressures, ~300 bar (green data points and fitted line) and 500 bar (blue data points and fitted line), fit to Eq. (3), with the simultaneous fit of both data sets shown by the solid magenta line. The rate constants $k_{He\mu}$ are given by the slopes: $k_{He\mu} = (3.74 \pm 0.50) \times 10^{-16}$ cm^3 molecule^{-1} s^{-1} at 300 bar, $(4.09 \pm 0.66) \times 10^{-16}$ cm^3 molecule^{-1} s^{-1} at 500 bar, with the combined value, $k_{295.5K} = (3.85 \pm 0.40) \times 10^{-16}$ cm^3 molecule^{-1} s^{-1}. Though errors on the determination of $[H_2]$ are shown, these have little impact on the fit. The errors on the plotted points and on the rate constants determined from the slopes are statistical only. Note the value of λ_b from the $[H_2] = 0$ intercept, ~0.05 μs^{-1}, close to zero on the plotted scale.

with $[H_2] = 0.87 \times 10^{20}$ molecules cm^{-3} at 405 K and 0.42×10^{20} molecules cm^{-3} at 500 K (both at 500 bar), that the initial amplitudes $A_{He\mu}$ are close to the maximum value seen in Fig. 4 (top), due to a much reduced level of competitive μ^- capture at these lower H_2 concentrations. Note also that the relaxation rates, $\lambda_{He\mu}$, due to the Heμ + H_2 reaction, are considerably faster at the higher temperatures.

In the μSR technique employed,[4,12,31,43,48] there is only one muon in the target at a given time, so the reaction exhibits pseudo first-order kinetics.[48] The measured relaxation rate constant, $\lambda_{He\mu}$, is primarily due to dephasing of the diamagnetic product HeμH formed from the Heμ + H_2 abstraction reaction. It is related to the rate constant of interest, $k_{He\mu}$, by

$$\lambda_{He\mu} = \lambda_b + k_{He\mu}[H_2], \quad (3)$$

where λ_b is a background relaxation independent of the H_2 reactant, due to magnetic field inhomogeneity or impurities in the dopant NH_3 or He gas, including possible reaction of the Heμ atom with the NH_3.

The relaxation rate constants vs. H_2 concentration were measured at two total pressures, near 300 bar and 500 bar, at 295.5 K, and are plotted in Fig. 6. Figure 7 plots similar data at 405 and 500 K from measurements at 500 bar only. Although there is a hint of a faster relaxation in the 500 bar data of Fig. 6 at 295.5 K, giving $k_{He\mu} = (4.09 \pm 0.66) \times 10^{-16}$ cm^3 molecule^{-1} s^{-1} (dashed blue fitted line) vs. $(3.74 \pm 0.50) \times 10^{-16}$ in the same units at 300 bar (dashed green fitted line), these slopes are within uncertainties, as are the individual determinations of $\lambda_{He\mu}$. A simultaneous fit to both data sets (magenta fitted line) in Fig. 6 gives $k_{295.5\,K} = (3.85 \pm 0.40) \times 10^{-16}$ cm^3 molecule^{-1} s^{-1}. It is noted that no density dependence is expected for the Heμ + H_2 abstraction reaction. Accordingly, the higher temperature data (Fig. 7) were taken at 500 bar pressure only, which provides a better muon stopping density at these temperatures. The fitted rate constants from the slopes in Fig. 7 are: $k_{405\,K} = (7.06 \pm 0.87) \times 10^{-15}$ cm^3 molecule^{-1} s^{-1} and $k_{500\,K} = (3.56 \pm 0.56) \times 10^{-14}$ cm^3 molecule^{-1} s^{-1}. The quoted uncertainties are statistical only, from the MINUIT (Ref. 51) fits to the data. Although these signals are weak and difficult to fit, the results were remarkably stable to parameter variations and choices for initial guesses. Still, some systematic error can be expected and this is assessed below.

Molecular oxygen is a common impurity in most gases, although usually at low levels. Being paramagnetic, O_2

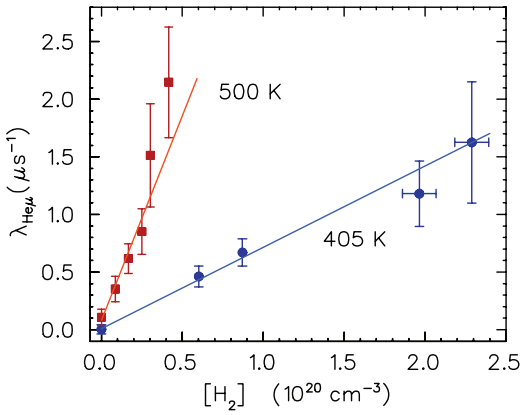

FIG. 7. Relaxation rates vs. $[H_2]$ for the Heμ + H_2 reaction rate at 405 K (lower blue data points and fitted line) and 500 K (upper red data points and fitted line). See also caption of Fig. 6. Accurate H_2 partial pressures were measured to 0.5% with a Baratron manometer over the whole concentration range for the data at 500 K and for the lower pressures at 405 K, and these uncertainties give error bar smaller than the plotted points. The total pressure in each case is 500 bar (He). Rate constants, determined from the slopes [Eq. (3)] are: $k_{405\,K} = (7.06 \pm 0.87) \times 10^{-15}$ cm^3 molecule^{-1} s^{-1} and $k_{500\,K} = (3.56 \pm 0.56) \times 10^{-14}$ cm^3 molecule^{-1} s^{-1}; the uncertainties are statistical only. The larger intercept giving λ_b ~0.09 μs^{-1} at 500 K is believed due to an enhanced reaction of Heμ with NH_3, added as a dopant to produce muonic He. See the discussion in Sec. III of the text.

can cause electron spin exchange (SE) with Mu, leading to depolarization of the muon spin as a consequence of the subsequent muon-electron hyperfine interaction[52] and hence an increase in the muon relaxation rate. The Mu + O_2 SE reaction has been well studied[4,52] and it has been established that the thermally averaged SE cross section is independent of temperature above 90 K. A similar effect can be expected for Heμ + O_2. Although the target vessel and plumbing were thoroughly leak checked and always left at positive pressure, some trace amount of O_2 might still have been present in the system.

The bulk of the gas in the target vessel at all temperatures and particularly at 405 K and 500 K was the He moderator, in which the $(He\mu)^+$ ion is initially formed. This was UHP grade with a stated O_2 impurity of <1 ppm and was also "gettered" with a commercial filter. Still, at the high He pressures used, a trace amount of O_2 may have been present, along with similar residual levels in the target and plumbing. Both could contribute to the background relaxation rate λ_b in Eq. (3). In contrast any O_2 present in the hydrogen reactant, which was of higher purity (<0.1 ppm), could be a source of systematic error and is commented on later.

At the temperatures of interest the relaxation rate from the Mu + H_2 reaction is too slow to be seen,[8,9] so measurements of the relaxation rate of Mu precession were carried out (with μ^+) both before and after each negative muon run as independent tests of λ_b. These tended to give a smaller value for the Mu relaxation after each long μ^- run, as compared to its value before, which we attribute to scavenging of O_2 impurity by the dopant NH_3, due to the presumed 2 NH_3 + 3/2 $O_2 \rightarrow N_2$ + 3 H_2O reaction. This is also indicated by the unusually low values found for λ_b seen in the intercepts at 295.5 K in Fig. 6 and at 405 K in Fig. 7, which were most probably then due to field inhomogeneity. Reaction of Heμ with NH_3 may also be contributing here, and most likely dominates at 500 K, where λ_b is noticeably higher at ~0.09 μs^{-1}, in accord with the high activation energy of ~10 kcal/mol for the analogous H + NH_3 abstraction reaction.[53,54]

IV. THEORETICAL METHODS

IV.A. Potential energy surfaces

For very accurate work we must distinguish the BO PES from the Born–Huang (BH) one.[55] The BO PES equals the electronic energy plus the nuclear repulsion at fixed nuclear positions and hence is independent of nuclear masses. The BH PES is obtained by including the Born–Oppenheimer diagonal correction (BODC), which depends on the nuclear masses but is small. The BH surface for each isotopic combination is the sum of an isotope-independent BO PES and an isotope-dependent BODC. All dynamical calculations presented in this paper itself use the BH PES (calculations on the BO PES are reported in supplementary material).[56]

The BO surface is a fit[57] to complete configuration interaction (CCI) results to yield a global PES for H + H_2. The CCI results were obtained by carrying out multireference configuration interaction (MRCI) calculations that are within 1 μE_h of the full configuration interaction (FCI) limit and extrapolating them to the complete basis set limit with a many-body basis set extrapolation scheme,[58] yielding an accuracy that is typically within ~0.01 kcal/mol of the exact BO potential. The BO saddle point energy on this PES is 9.602 kcal/mol, which compares well with the best estimate[59] of 9.608 kcal/mol obtained from many-body basis set extrapolations using basis sets as large as octuple zeta in quality (this estimate also agrees with the best quantum Monte Carlo estimate[60] of 9.608 ± 0.001 kcal/mol).

A key assumption in these calculations is that a $He\mu^+$ particle may be approximated as a heavy H pseudo-nucleus, with mass 4.115 amu, and thus that Heμ + H_2 and ^4H + H_2 may be treated as having the same PES. The mean radius of the muon 1*s* orbital of 0.00373 a_0 is more than a factor of 400 smaller than the mean 1*s* electron radius of 1.50016 a_0,[61] so it is reasonable to expect that the muon provides nearly perfect screening of one unit of nuclear charge for the electron. Further support for this assumption may be seen in calculations[61] of the Heμ hyperfine coupling constant, ν_0(Heμ), where a pseudonucleus approximation yields 4464.00 ± 0.05 MHz, an explicit treatment of the muon orbital yields 4464.87 ± 0.05 MHz, and the experimental value[28] is 4465.004 ± 0.029 MHz. These data may be compared with the hyperfine coupling constant for the Mu atom of 4463.302 MHz,[30] which would be the expected result for Heμ if the muon orbital was approximated as a delta function.

An approximate estimate of the possible error due to the pseudo-nucleus approximation for the Heμ + H_2 reaction was obtained using a pseudopotential (PP) approach. In particular, a local potential was added to a He atom that describes the Coulomb interaction between a single electron and the +2 nuclear charge screened by a closely held, negatively charged muon. A linear combination of five Gaussians as a function of the electron-nuclear distance r was accurately fit to the expression $(1/r + \alpha/2)e^{-\alpha r}$, in Hartree atomic units, where $\alpha = 2\ Z\ m_\mu = 827.07306\ a_0^{-1}$. The usual long-range $-1/r$ Coulombic term was then added to this sum. The resulting pseudopotential behaves like $-2/r$ near $r = 0$ and $-1/r$ at distances outside the tight orbit of the negative muon. To determine if Heμ really does behave similarly to a hydrogen atom, a series of barrier height calculations as a function of basis set was carried out for both Heμ + H_2 (using the PP model for Heμ) and H + H_2 using the same near-FCI quality wave functions as those used in the original determination of the CCI surface. The results are shown in Table I, where we begin with a basis set consisting of the completely uncontracted H-atom aug-cc-pV5Z set and add to this initial basis additional even-tempered tight functions up to $11s12p12d11f$. These results show that the BO barrier height on the Heμ + H_2 surface is identical to the H + H_2 one to within ~0.001 kcal/mol. Energetic differences of this magnitude will lead to negligible differences in the calculated rate constants.

Having confirmed the validity of treating Heμ as an isotope of H, a BODC correction surface[62] was added to the CCI BO surface to yield the BH surface. The fitted diagonal correction surface leads to an increase in the barrier height (9.602 kcal/mol on the BO PES) relative to asymptotically separated H_2 of 0.1535, 0.1399, 0.3697, and 0.1328 kcal/mol for H + H_2, D + H_2, Mu + H_2, and Heμ + H_2, respectively;

TABLE I. Comparison of total energies (E_h) and barrier heights (kcal/mol) of H + H_2 and Heμ + H_2 as a function of basis set at a near-FCI level of theory. The Heμ + H_2 results used a pseudopotential approach as described in the text.

	H + H_2	H–H_2	ΔE_b	Heμ + H_2	Heμ–H_2	ΔE_b	$\Delta(\Delta E_b)$
Uncontr. AV5Z[a]	−1.674259	−1.658919	9.6261	−1.674248	−1.658906	9.6273	0.0012
+11*s*	−1.674273	−1.658933	9.6265	−1.674261	−1.658919	9.6274	0.0009
+11*s*12*p*	−1.674285	−1.658943	9.6274	−1.674273	−1.658929	9.6284	0.0010
+11*s*12*p*12*d*	−1.674301	−1.658956	9.6290	−1.674288	−1.658942	9.6300	0.0010
+11*s*12*p*12*d*11*f*	−1.674316	−1.658969	9.6306	−1.674304	−1.658955	9.6315	0.0009

[a]An uncontracted aug-cc-pV5Z basis set; basis functions listed on later lines are added to this basis.

electronic structure benchmarks[59] for H + H_2, D + H_2, and Mu + H_2, agree with these values to within 0.0003, 0.0004, and 0.0026 kcal/mol, respectively. In prior calculations[41] for the rate constants of D + H_2 and H + D_2, the effect of the BODC on the thermal rate constants was estimated by a simple barrier height correction scheme, i.e.,

$$k^{\mathrm{BH}}(T) \approx \exp(-\Delta_{\mathrm{barrier}}/k_B T)\, k^{\mathrm{BO}}(T), \tag{4}$$

where $\Delta_{\mathrm{barrier}}$ is the difference between the BH and BO barrier height. This approximate correction scheme led to markedly improved agreement between theory and experiments. The recent availability of a functional representation[62] of the BODC now obviates the need for such approximate corrections. In the following, in addition to calculations for Heμ + H_2, we will also present new calculations for Mu + H_2 and D + H_2 on the BH surface so that isotope ratios can be calculated using a consistent level of theory.

IV.B. Accurate quantum calculations

The QM calculations employed the outgoing wave variational principle[63–65] to calculate cumulative reaction probabilities[66] (CRPs) for both the BO and the BH surfaces. The calculations were performed on a grid of total energies (E) for all significant values of the total angular momentum, J, parity, P, and homonuclear diatom symmetry, $S = (-1)^j$ where j is the H_2 rotational quantum number. Checks of the numerical uncertainty were performed at selected values of E, J, P, and S by simultaneously varying a sufficient subset of basis set parameters and numerical parameters needed to demonstrate convergence; these tests indicate that the CRPs are accurate to within a few tenths of a percent, and we expect that the J-summed CRPs and the thermal rate constant (which are discussed next) are accurate to better than 0.2%.

The thermal rate constant as a function of the temperature, T, may be expressed as

$$k(T) = \sum_{J=0}^{\infty} (2J+1) k_J(T), \tag{5}$$

where, for a bimolecular collision A + BC, we have[67]

$$k_J(T) = \frac{\int_0^\infty dE\, N_J(E)\, e^{-E/k_B T}}{h \Phi_{\mathrm{rel}}(T) Q_A(T) Q_{BC}(T)}, \tag{6}$$

where h is Planck's constant, $Q_A(T)$ is the partition function of A, $Q_{BC}(T)$ is the partition function of BC, $\Phi_{\mathrm{rel}}(T)$ is the partition function per unit volume of the relative translation of A with respect to BC, i.e.,

$$\Phi_{\mathrm{rel}}(T) = (2\pi \mu_{\mathrm{A-BC}} k_B T)^{3/2} / h^3, \tag{7}$$

where $\mu_{\mathrm{A-BC}}$ is the A–BC reduced mass, and $N_J(E)$ is the CRP for total angular momentum J. The $N_J(E)$ include factors of $(2I + 1)$, where I is the nuclear spin, to account for nuclear spin statistics

$$N_J(E) = \sum_{P=-1}^{+1} N_{JP}^{(S=+1)}(E) + 3 \sum_{P=-1}^{+1} N_{JP}^{(S=-1)}(E), \tag{8}$$

as does the H_2 partition function, where para-H_2 has even symmetry [$(S = +1)$ and $(I = 0)$] and ortho-H_2 has odd symmetry [$(S = -1)$ and $(I = 1)$], and $N_{JP}^{(S)}$ indicates the CRP restricted to specific values of J, P, and S.

It will be convenient to also consider the JP-summed CRPs

$$N^{(S)}(E) = \sum_{J=0}^{\infty} \sum_{P=-1}^{+1} (2J+1) N_{JP}^{(S)}(E), \tag{9}$$

and the CRPs summed over J, P, and S, i.e.,

$$N(E) = N^{(S=+1)}(E) + 3N^{(S=-1)}(E). \tag{10}$$

Equations (5) and (6) may also be written as

$$k(T) = \frac{\int_0^\infty dE\, N(E)\, e^{-E/k_B T}}{h \Phi_{\mathrm{rel}}(T) Q_A(T) Q_{BC}(T)}. \tag{11}$$

The quadrature in Eq. (11) was evaluated by first fitting the logarithm of $N(E)$ on the calculated energy grid with a spline function to get data at the quadrature nodes. A small contribution to this quadrature from energies above the maximum grid value was obtained by fitting the highest energy data to a polynomial and extrapolating. At the temperatures of experimental interest here and for all tabulated temperatures for the Mu + H_2 and D + H_2 reactions, these extrapolated contributions are negligible, but they are as much as 5.4% at $T = 1000$ K for the Heμ + H_2 reaction.

For the Heμ + H_2 reaction on the BH PES, CRPs were calculated in the energy range of 0.28–1.20 eV (relative to the classical minimum of Heμ + H_2) at an interval of 0.02 eV. After being summed over J and P, the values for the ortho $(S = -1)$ and para $(S = +1)$ CRPs for $E \geq 0.48$ eV display a mean unsigned deviation of 0.04% and a maximum deviation of 0.15%; at lower energies the ratio of the ortho to para CRPs is 1.004 at 0.42 eV, 0.934 at 0.34 eV, 0.385 at 0.30 eV, and 0.000 at 0.28 eV (where there are no open odd j channels). Over the range of temperatures (200–1000 K) considered here, the Boltzmann weighting of Eq. (11) leads to nearly

negligible contributions from $E < 0.40$ eV; thus, the approximation $N^{(S=+1)}(E) \approx N^{(S=-1)}(E)$, that we have used in past calculations,[41,67] leads to uncertainties in the rate constants of less than 0.1%. This near equivalence of the ortho and para CRPs over a wide energy range is consistent with the reactive flux being mediated by transition states[68–72] that lie near the saddle point region and that thus have no dependence on the homonuclear symmetry number.

For the D + H_2 reaction, calculations were performed on the BH PES in the energy range 0.28–1.8 eV at an interval of 0.02 eV. As noted above, the D + H_2 reaction has been considered previously[41] on the BO PES, and rate constants on the BH surface were estimated with an approximate barrier correction by using Eq. (4). This approximation predicts rate constants that are systematically slightly lower than those for the accurate BH PES; the BH rate constants are higher than the approximate results by 19%, 7.9%, 2.4%, and 1.1% at 200 K, 300 K, 600 K, and 1000 K, respectively. A more detailed comparison of the approximate results obtained using Eq. (4) and the results on the BH PES is presented in the supplementary material. For the Mu + H_2 reaction, calculations were performed on the BH PES in the energy range 0.60–2.0 eV at an interval of 0.02 eV. Values of 207.678, 1837.153, 3671.483, and 7502.046 m_e were used for the masses of Mu, H, D, and Heμ, respectively.

IV.C. Separable rotation approximations

Separable rotation approximations (SRA) (Refs. 64 and 70–75) have a long history,[73,74] with many variations and are sometimes called J-shifting approximations.[67,75–80] The high accuracy of the SRA has been demonstrated previously[67] for the D + H_2 reaction, and as part of the present work we found that for the Heμ + H_2 reaction on the BH PES its use yields agreement within 0.6% of the accurate QM calculations (see supplementary material). Given this high accuracy we use the SRA for calculations on the BO surface for the Heμ + H_2 and D + H_2 reactions in order to affordably calculate KIEs for $k_D/k_{He\mu}$ that can be compared with the analogous values on the BH PES.

The SRA, when applied to a transition state, assumes that the energy of overall rotation in the transition state region is unavailable for barrier crossing so CRPs at one value of J may be approximated from values at another J by

$$N_J\left(E + E_J^{\mathrm{VTS}}\right) \approx N_{J'}\left(E + E_{J'}^{\mathrm{VTS}}\right), \tag{12}$$

where E_J^{VTS} denotes the energy sequestered in overall rotation at the transition state for a given value of J. Within this approximation, the rate constant may be obtained using data at a single value of J via

$$k(T) = Q_{\mathrm{rot}}^{\mathrm{VTS}}(T) \exp\left(E_{J'}^{\mathrm{VTS}}/k_B T\right) k_{J'}(T), \tag{13}$$

where

$$Q_{\mathrm{rot}}^{\mathrm{VTS}}(T) = \sum_{J=0}^{\infty} (2J+1) \exp\left(-E_{J'}^{\mathrm{VTS}}/k_B T\right). \tag{14}$$

In the present calculations we approximate E_J^{VTS} differently at each temperature using

$$E_J^{\mathrm{VTS}} \approx B^{\mathrm{eff}}(T) J(J+1), \tag{15}$$

where the effective rotation constant, $B^{\mathrm{eff}}(T)$, is chosen so that the SRA predicts the rate constant $k_{J''}(T)$ exactly based on the value of $k_{J'}(T)$. This leads to the expression[67]

$$B^{\mathrm{eff}}(T) = \frac{k_B T \ln[k_{J''}(T)/k_{J'}(T)]}{J'(J'+1) - J''(J''+1)}. \tag{16}$$

In the high-temperature limit the value of $B^{\mathrm{eff}}(T)$ is close to the value $\hbar^2/2I^{\ddagger}$, where $I^{\ddagger}$ is the moment of inertia at the saddle point. The use of an effective rotation constant has been shown[67] to lead to very high accuracy over a wide range of temperatures when compared to the summation over all values of J. In the present calculations we adopt $J' = 6$ and $J'' = 9$ for use in Eqs. (13)–(16).

In addition to the accurate QM calculations discussed in Sec. IV.B, thermal rate constants, within the SRA approximation, were obtained for both the BH and BO PES for the Heμ + H_2 reaction and the D + H_2 reaction. For both reactions we approximate the CRPs of the ortho and para symmetries as being equal (for the temperatures considered here, this introduces negligible additional inaccuracy in the computed rate constants).

IV.D. Variational transition state theory

Because accurate QM calculations are only affordable for small systems it is useful to benchmark approximate methods that scale better with the system size, specifically variational transition state theory.[81] The VTST calculations presented here employed methods described in detail in Refs. 7, 82–89 and were carried out by using ABCRATE,[87] a computer program for the calculation of atom-diatom reaction rates for systems, such as the H + H_2 reaction, that have collinear-dominated reaction paths. Calculations were performed on the BH PES. Specifics of the theory and implementation of VTST can be found in the references given above. Here we only present sufficient details to allow the calculations to be reproduced.

We used improved canonical variational theory (ICVT) (Ref. 83) with multidimensional tunneling contributions. Partition functions for the vibrational and rotational modes were approximated as being separable. Rotational partition functions were computed using the quantized rigid rotor approximation. The one bound stretching vibrational mode (the other stretch mode is unbound along the reaction coordinate) was treated as uncoupled from the bending modes in curvilinear coordinates. The ground-state energy level was computed using the WKB approximation,[7] while excited-state energies were computed using the Morse I (Ref. 90) approximation. Curvilinear coordinates were also used to describe the bending motions, and the two bending modes were treated as coupled using the centrifugal oscillator approach,[86,91] where the potential for the bending motion was approximated by a harmonic-quartic potential, for which the parameters were fitted to reproduce the WKB ground-state energy level for the one-dimensional bend vibration. The

effect of multidimensional quantum mechanical tunneling and nonclassical reflection was computed using the least-action tunneling (LAT) method, which was called the least-action ground-state (LAG) method in the original paper.[84]

Variational transition state theory provides a convenient approach to analyze the factors controlling KIEs and gain more insight into the features of the PES that most influence the rate constants.[92,93] The KIE, which is the ratio of rate constants for the different isotopic masses, can be expressed as a product of factors in the rate expressions for the two isotopically different reactions.[92,93] In VTST we can write the KIE as the product of the following factors:

- η_{trans}—the ratio of the reactant partition functions for relative translational motion;
- η_{rot}, η_{str}, and η_{bend}—the ratio of rotational, stretch, and bend partition functions (note that since we use ICVT, the partition functions of the variational transition states are the improved ones);
- η_{tun}—the ratio of the transmission coefficients that account for tunneling and nonclassical reflection;
- η_{pot}—the contribution to the KIE from the difference in potential energy at the variational transition state, the location of which depends on the isotopic masses.

By convention, KIEs are reported with the rate constant for the lighter mass combination in the numerator, which is expected to give a KIE that is greater than 1 for normal cases. A KIE of less than unity is referred to as "inverse."

IV.E. Fitting the temperature dependence of the rate constants

The theoretical rate constants, both the accurate quantal ones and the VTST ones, may be calculated at as many temperatures as desired with negligible expense (in the case of the QM results, calculation of the CRPs involves significant cost, but given these data the cost of the Boltzmann weighting to get $k(T)$ at a large number of temperatures is insignificant); thus, we do not need to rely on fits for these quantities. However, the various experimental data sets all display significant statistical uncertainties in addition to possible systematic errors. Numerical fits of such data sets can greatly reduce the statistical uncertainties and allow for more meaningful comparisons to theory. Whenever sufficient experimental data are available, fits of rate constant data in Secs. V and VI will be obtained with a functional form recommended previously[94] and given by

$$k(T) = C_1 T^{C_2} \exp\left(-\frac{C_3(T + C_4)}{k_B(T^2 + C_4^2)}\right), \tag{17}$$

where C_1, C_2, C_3, and C_4 are fitting parameters chosen to minimize the root-mean-square error when $\ln k$ is fitted as a function of $1/T$. The experimental Arrhenius activation energy, E_a, which is defined as

$$E_a(T) = -k_B \frac{d\ln k}{d(1/T)}, \tag{18}$$

may then be calculated from this expression as

$$E_a(T) = C_2 k_B T + C_3 \frac{T^4 + 2C_4 T^3 - C_4^2 T^2}{(T^2 + C_4^2)^2}. \tag{19}$$

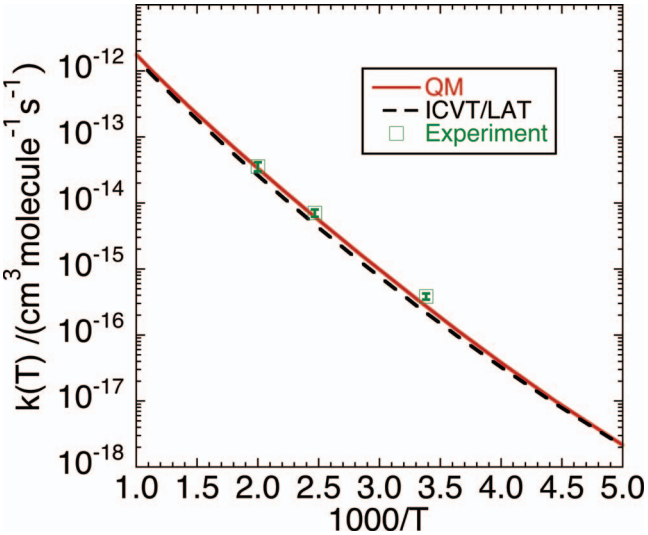

FIG. 8. Comparison of experimental and theoretical thermal rate constants, $k_{\text{He}\mu}(T)$, for the $\text{He}\mu + \text{H}_2$ reaction as a function of temperature. The experimental error bars shown are statistical only, determined from the fits to the relaxation rates shown in Figs. 6 and 7. The temperature uncertainties are ±1.5 K at 295.5 and 500 K and ±1.0 K at 405 K and are too small to plot. See the discussion in Sec. III of the text.

The activation energies reported for theoretical methods are obtained by accurate finite difference of closely spaced rate constants. We note that all fits using Eq. (17) were of excellent quality and that the quoted results do not deviate significantly from those obtained from alternative fits where $\ln k$ is fitted as a low-order polynomial in $1/T$.

V. COMPARISON OF EXPERIMENTAL AND THEORETICAL RESULTS FOR THE $\text{He}\mu + \text{H}_2$ RATE CONSTANTS

The experimental rate constants, $k_{\text{He}\mu}$, as reported in Sec III.B, are plotted vs. inverse temperature, along with the results from theory, in the Arrhenius plot of Fig. 8. The visible error bars are predominately statistical, determined from the fits illustrated in Figs. 6 and 7. Uncertainties for the measured temperatures, given earlier, are at most 1.5 K and barely exceed the size of the plotted points. (These temperature errors are *much* less than those in the 1987 report of the $\text{Mu} + \text{H}_2$ reaction rate.[9] In that study, the high temperatures demanded by the slow reaction rates, up to 900 K, dictated a target of very different design.)

The Arrhenius plot of Fig. 8 comparing the experimental rate constants $k_{\text{He}\mu}$ with theory for the $\text{He}\mu + \text{H}_2$ reaction is the central result of the present study. The accurate quantum mechanical calculations are essentially in perfect agreement with the experimental data at 500 K, where they are well within experimental error. Good agreement with experiment is also found at 405 K, where the QM calculations are within 15% of experiment, falling just below the 1σ (statistical) error bar shown. However, at 295.5 K the QM result of 2.71×10^{-16} cm^3 molecule^{-1} s^{-1} is 30% below experiment (Table II), a surprisingly large disagreement given that the level of agreement between theory and several experiments[37–40,95–97] for both $\text{H} + \text{D}_2$ and $\text{D} + \text{H}_2$ is within ~10% over much wider temperature ranges,[41] and

TABLE II. Comparisons between theory and experiment for $k_{He\mu}$(cm^3 $molecule^{-1}$ s^{-1}).

T(K)	k_{exp}[a]	k_{QM}[b]	k_{VTST}[c]	κ[d]
200	...	2.15×10^{-18}	2.09×10^{-18}	35.1
250	...	3.83×10^{-17}	3.27×10^{-17}	8.5
295.5	$(3.85 \pm 0.55) \times 10^{-16}$	2.71×10^{-16}	2.16×10^{-16}	4.3
300	...	3.21×10^{-16}	2.54×10^{-16}	4.1
350	...	1.59×10^{-15}	1.23×10^{-15}	2.7
400	...	5.51×10^{-15}	4.24×10^{-15}	2.1
405	$(7.06 \pm 1.12) \times 10^{-15}$	6.14×10^{-15}	4.73×10^{-15}	2.1
450	...	1.48×10^{-14}	1.15×10^{-14}	1.8
500	$(3.56 \pm 0.66) \times 10^{-14}$	3.34×10^{-14}	2.62×10^{-14}	1.6
550	...	6.58×10^{-14}	5.24×10^{-14}	1.5
600	...	1.17×10^{-13}	9.44×10^{-14}	1.4
650	...	1.92×10^{-13}	1.57×10^{-13}	1.3
700	...	2.96×10^{-13}	2.45×10^{-13}	1.3
800	...	6.10×10^{-13}	5.17×10^{-13}	1.2
900	...	1.09×10^{-12}	9.46×10^{-13}	1.2
1000		1.77×10^{-12}	1.56×10^{-12}	1.1

[a]The errors on the experimental rate constants expanded to include systematic error that has been estimated at 10%. See discussion in the text.
[b]The accurate quantum theory calculations of rate constants $k_{He\mu}$ for Heμ + H_2.
[c]As in footnote b but for VTST ICVT/LAT calculations.
[d]The tunneling factor is defined as the ratio of the ICVT/LAT calculated rate constant with the LAT tunneling path to the ICVT rate constant alone, in the absence of tunneling.

that quantum theory also yields excellent agreement with the earlier Mu + H_2 rate constant measurements as discussed below. The ICVT/LAT calculations for Heμ + H_2 are in good agreement with the accurate QM data, although as much as 23% lower over the temperature range plotted.

If the experimental Heμ + H_2 rate constants are fit to a simple Arrhenius form [there is insufficient data to use Eq. (17)] the Arrhenius activation energy is found to be 6.45±0.32 kcal/mol; this can be compared to accurate QM values of 6.51, 7.03, and 7.33 kcal/mol at 295.5, 405, and 500 K, respectively. (If the QM results were fit to a simple Arrhenius expression over the 295.5–500 K temperature range then the estimated E_a would be 6.9 kcal/mol).

The Heμ + H_2 rate constants are also compared for the three temperatures of the experiment, with the experimental uncertainties expanded to include potential systematic errors (discussed below) as well as over a wider range of temperatures in Table II. Also shown in this table are transmission coefficients (κ) at each temperature from the ICVT/LAT calculations. We note that even for this heaviest of H-atoms there is still an appreciable tunneling effect for the Heμ + H_2 reaction at the lower temperatures, which can be inferred also from the extent of Arrhenius curvature in Fig. 8. This feature is discussed further in comparison with KIEs for the D + H_2 and Mu + H_2 reactions below.

VI. DISCUSSION: COMPARISONS OF EXPERIMENT TO THEORY

VI.A. Theory vs. experiment for the Heμ + H_2 reaction rate

The level of disagreement between theory and experiment noted above for the Heμ + H_2 reaction at 295.5 K (Fig. 8 and Table II) leads us to explore possible reasons, including systematic experimental error, for this discrepancy. The data are generally difficult to fit, due to small-amplitude signals, as discussed earlier. Sixteen parameters are varied in fitting the data to Eq. (2), and there are correlations between some of these, which might well be enhanced in the case of fitting to small-amplitude signals. In particular, at 295.5 K the signal amplitudes are reduced further by competitive μ^- capture on H_2 at the relatively high concentrations required, as can be seen in Fig. 4. However, even though these signal amplitudes are weak, the fits at all temperatures were surprisingly robust to changing initial guesses over wide margins and also to small changes in the Heμ lifetime, which is not as well known as for other muonic atoms.[50] The effects of these kinds of changes were small, with the fitted results generally being within 10% of the statistical errors given above (and plotted in Fig. 8).

Moreover, at 295.5 K there are nine data points in total (Fig. 6) from two different moderator pressures obtained in separate run periods a year apart, and, as previously remarked, with rate constants that agree within statistical errors, so it is unlikely that there is a singular source of systematic error here. Although there is a hint of a moderator pressure dependence from the separate fits shown in Fig. 6, with the 300 bar value of $k_{He\mu} = (3.74 \pm 0.50) \times 10^{-16}$ cm^3 $molecule^{-1}$ s^{-1} (green fitted line) being in slightly better agreement with theory, this is not viewed as significant. The result given in Sec. III.B from fitting the complete data set, $k_{295.5} = (3.85 \pm 0.40) \times 10^{-16}$ cm^3 $molecule^{-1}$ s^{-1}, has a weighted statistical error of only ±10%, much less than the ~30% lower value for $k_{He\mu}$ calculated by the quantum theory at this temperature. Furthermore, although it is true that the signal amplitudes are weaker at 295.5 K, they are not all that much stronger at higher temperatures where the agreement between theory and experiment is essentially within errors, supporting a claim that the fitting procedure is sound.

In addition to parameter variations commented on above, another method to try to assess the level of systematic error in the experiment is to examine the reproducibility of the fitted results from different run periods and from different methods of analysis. These kinds of variations gave consistent results to within 10% on average, though there were larger excursions for some specific changes.

A further possible source of error here is spin exchange between the muonic He atom and O_2 impurity present in the hydrogen *reactant*, which could be a source of systematic error, increasing the muon relaxation rate $\lambda_{He\mu}$ due to the depolarization of the muon spin arising from an electron "spin flip" in Heμ.[4,52] Though the H_2 gas was of high purity, with a stated O_2 content of <0.1 ppm, any effect due to SE would have the biggest impact at 295.5 K, where the H_2 densities were highest. Mu spin precession experiments both in the presence of and in the absence of H_2 showed that relaxation rates decreased markedly over time, to a common value of ~0.05 μs^{-1}, due to the scavenging of O_2 by the NH_3 + O_2 reaction mentioned earlier. This corresponds to the λ_b intercepts of Figs. 6 and 7. There are indications that the decline was greatest for the highest concentrations of H_2, but still the total decrease for Mu in each

TABLE III. Rate constants (cm^3 $molecule^{-1}$ s^{-1}) and KIEs for the Heμ + H_2, D + H_2, and Mu + H_2 reactions.

T(K)	$k_{He\mu, QM}$[a]	$k_{He\mu, LAT}$[b]	$k_{D, QM}$[c]	$k_{D, LAT}$[d]	$k_{Mu, QM}$[e]	$k_{Mu, LAT}$[f]	$k_{D, QM}/k_{He\mu, QM}$	$k_{Mu, QM}/k_{He\mu, QM}$
200	2.15×10^{-18}	2.09×10^{-18}	2.20×10^{-18}	2.82×10^{-18}	7.00×10^{-24}	1.73×10^{-24}	1.022	3.25×10^{-6}
250	3.83×10^{-17}	3.27×10^{-17}	3.79×10^{-17}	4.11×10^{-17}	1.34×10^{-21}	3.95×10^{-22}	0.989	3.49×10^{-5}
300	3.21×10^{-16}	2.54×10^{-16}	3.19×10^{-16}	3.06×10^{-16}	6.44×10^{-20}	2.30×10^{-20}	0.994	2.01×10^{-4}
350	1.59×10^{-15}	1.23×10^{-15}	1.60×10^{-15}	1.43×10^{-15}	1.23×10^{-18}	5.17×10^{-19}	1.008	7.74×10^{-4}
400	5.51×10^{-15}	4.24×10^{-15}	5.63×10^{-15}	4.84×10^{-15}	1.23×10^{-17}	5.84×10^{-18}	1.021	2.24×10^{-3}
450	1.49×10^{-14}	1.15×10^{-14}	1.53×10^{-14}	1.30×10^{-14}	7.75×10^{-17}	4.02×10^{-17}	1.033	5.22×10^{-3}
500	3.34×10^{-14}	2.62×10^{-14}	3.49×10^{-14}	2.94×10^{-14}	3.47×10^{-16}	1.93×10^{-16}	1.043	1.04×10^{-2}
550	6.58×10^{-14}	5.24×10^{-14}	6.92×10^{-14}	5.84×10^{-14}	1.20×10^{-15}	7.08×10^{-16}	1.051	1.82×10^{-2}
600	1.17×10^{-13}	9.44×10^{-14}	1.24×10^{-13}	1.05×10^{-13}	3.42×10^{-15}	2.11×10^{-15}	1.058	2.92×10^{-2}
650	1.92×10^{-13}	1.57×10^{-13}	2.04×10^{-13}	1.75×10^{-13}	8.38×10^{-15}	5.37×10^{-15}	1.063	4.36×10^{-2}
700	2.96×10^{-13}	2.45×10^{-13}	3.16×10^{-13}	2.73×10^{-13}	1.82×10^{-14}	1.20×10^{-14}	1.067	6.13×10^{-2}
800	6.10×10^{-13}	5.17×10^{-13}	6.56×10^{-13}	5.76×10^{-13}	6.48×10^{-14}	4.51×10^{-14}	1.074	1.06×10^{-1}
900	1.09×10^{-12}	9.46×10^{-13}	1.18×10^{-12}	1.06×10^{-12}	1.77×10^{-13}	1.28×10^{-13}	1.079	1.62×10^{-1}
1000	1.77×10^{-12}	1.56×10^{-12}	1.92×10^{-12}	1.75×10^{-12}	3.99×10^{-13}	2.98×10^{-13}	1.083	2.25×10^{-1}

[a]Entries from Table II for the accurate QM rate constants for Heμ + H_2, $k_{He\mu, QM}(T)$.
[b]Entries from Table II for the ICVT/LAT rate constants of VTST for Heμ + H_2, $k_{He\mu, LAT}(T)$.
[c]Accurate QM rate constants for D + H_2, $k_{D, QM}(T)$.
[d]ICVT/LAT rate constants of VTST for D + H_2, $k_{D, LAT}(T)$.
[e]Accurate QM rate constants for Mu + H_2, $k_{Mu, QM}(T)$.
[f]ICVT/LAT calculations of VTST on the BH surface for the Mu + H_2 rate constants, $k_{Mu, LAT}(T)$.

case was well below the measured rates for Heμ and well below 30% of the rate. We are persuaded then that SE between Heμ and O_2 impurity in the hydrogen reactant cannot account for the disagreement seen between theory and experiment at 295.5 K, although it might contribute to some extent.

Another possibility, although remote, is that strongly interacting, but ultimately inelastic, collisions with H_2 lead to additional muon depolarization. This is a significant mechanism for muon (μ^+) depolarization in systems that display a collision complex such as in the Mu + CO addition reaction, which forms a bound $[MuCO \cdot]^*$ intermediate.[21] While such effects are likely to be small for systems that do not form stable complexes, they would likely be more important at lower temperatures, thus perhaps explaining at least part of the discrepancy between theory and experiment at 295.5 K.

Overall, we conclude that the best assessment of error in these experiments is found from the aforementioned determinations of the differences seen in fitted relaxation rates from parameter variations, different run periods or fitting methods, giving rise to an additional contribution to experimental error of ~10%. Combining this with the statistical error, the revised rate constants would be $k_{He\mu} = (3.85 \pm 0.55) \times 10^{-16}$ at 295.5 K, $(7.06 \pm 1.12) \times 10^{-15}$ at 405 K, and $(3.56 \pm 0.66) \times 10^{-14}$ at 500 K, all in units of cm^3 $molecule^{-1}$ s^{-1}. It is these values that are entered in Table II. Given these somewhat expanded uncertainties, the experimental and QM rate constants, $k_{He\mu}$, now overlap very well at the two highest temperatures of 405 and 500 K, with the rate constant at 500 K in complete agreement with the accurate QM results, as noted already in our short communication.[32] At the same time there appears to remain an appreciable level of disagreement between the accurate QM results and experiment at 295.5 K, with the lower limit of the data still 22% above theory. Possible sources of significant uncertainty in the QM calculations are essentially limited to the PES. The assumption that Heμ^+ may be treated as a pseudonucleus is well justified by the pseudopotential tests presented earlier, and the residual uncertainties in the BO PES of ~0.01 kcal/mol are not expected to lead to appreciable deviations in the rate constants at the temperatures considered in the experiments. Furthermore, the accurate QM KIEs for $k_D/k_{He\mu}$ shown in Table III are essentially identical for the BO and BH surfaces (see supplementary material for the BO data) which suggests that errors in the diagonal correction surface cannot be responsible for the remaining discrepancies between theory and experiment.

VI.B. Tests of variational transition state theory

The ICVT/LAT calculations for $k_{He\mu}$ on the BH surface are consistently below both theory and experiment at all temperatures (Table II, Fig. 8), although they are in reasonable agreement overall. The largest errors are 23% underestimates of the accurate QM results over the entire temperature range studied (a factor of five in T). This can be compared with the results for D + H_2 where VTST overestimates the QM rate by 29% at 200 K and has a maximum underestimate of 16% at 500 K. The largest uncertainties in the calculations arise from the approximate treatment of quantum mechanical tunneling and these uncertainties increase with decreasing T. The transmission coefficient, κ, which is the ratio of the ICVT/LAT rate constant to the ICVT rate constant that neglects tunneling and nonclassical reflection, is listed in the last column of Table II. It is largest at the lowest temperatures, increasing the rate constant for the Heμ + H_2 reaction by a factor of 35 at 200 K. There is no variational bound for the transmission coefficient, and it can be underestimated or overestimated.

VI.C. Isotopic comparisons: rate constants and KIEs for Heμ + H_2, D + H_2, and Mu + H_2

The present experimental results for the reaction rate constants of the heaviest H-atom isotope with hydrogen, the

Heμ + H_2 reaction, can now be compared with those for the lightest H-atom isotope, muonium, for the Mu + H_2 reaction;[9] these reactions differ by a factor of 36.1 in isotopic mass, and the results can also be compared with those for the D + H_2 reaction. The rate constants for all three reactions, Heμ + H_2, D + H_2, and Mu + H_2, are given over a wide range of temperatures in Table III for both the accurate QM and ICVT/LAT VTST calculations along with the QM-calculated KIEs for $k_D/k_{He\mu}$ and $k_{Mu}/k_{He\mu}$ given in the last two columns. Extensive tables are also provided in supplementary material comparing the QM calculations on the BO and BH PESs for the Heμ + H_2 and D + H_2 reactions.

There have been several earlier accurate QM studies[41,67,98] of the D + H_2 reaction on various BO PESs;[57,99–101] analysis of these results is already available,[41,67] and here we restrict attention to the results on the BH PES. There are five sets of experimental data available for the D + H_2 reaction.[37–40,42] The earliest three experiments all used similar techniques and we will compare the new QM rate constants to the aggregate of these three data sets, which consists of 51 measurements in the temperature range 178–745 K (we omit one measurement at 167 K that the authors[39] indicate did not meet all their criteria for reliability and which shows a very large discrepancy with both theory and a fit to the other measurements). The QM results have a mean unsigned percentage deviation (MUPD), i.e., $\langle 100|(k_{exp} - k_{QM})/k_{exp}|\rangle$, with the fitted data [using Eq. (17)] at the 51 temperature values of 6.0% and an MUPD with the raw data of 13.5%. The fourth experiment consists of shock tube measurements at 152 temperatures in the range T = 655–1979 K by Michael and Fisher.[40] The QM results have an MUPD with the fitted data of 22% and an MUPD with the raw data of 24%, with the experimental values typically being larger than the QM data. The 5th experiment consists of shock tube measurements at 50 temperatures in the range T = 1166–2112 K by Michael, Su, and Sutherland.[42] The QM results have an MUPD with the fitted data of only 1.5% and a MUPD with the raw data of 8.4%.

A single set of experimental data is available for the Mu + H_2 reaction consisting of 15 measurements in the range T = 473–843 K.[9] The QM rate constants have an MUPD with the fitted data at these points of 7.6% and an MUPD with the raw data of 9.8%. Two earlier QM studies[102–104] have been reported for the Mu + H_2 reaction; both employed the LSTH (Refs. 99, 105, and 106) BO PES, and both reported fair agreement with experiment. We have performed new accurate QM calculations on the LSTH BO PES, using the same procedures discussed earlier for the Mu + H_2 calculations on the BH PES, so that we can compare to these studies. The results of Schatz[102] employed a coupled states (CS) approximation and were estimated to have an uncertainty of ~30%. The CS data were tabulated at 15 temperatures in the range T = 200–1000 K and have an MUPD with the new accurate QM results of 18%, being too large by as much as 24% at 300 K and too small by as much as 34% at 1000 K (except for the T = 1000 K value all rate constants were accurate to within the stated 30% uncertainty). The later calculations of Tsuda *et al.*[103,104] were labeled as accurate QM results, but they fall short of this mark with the one tabulated value (their remaining data are only displayed graphically) at 745 K being 69% too high when compared to our converged results. A more complete comparison of the various LSTH rate constants is provided in supplementary material.

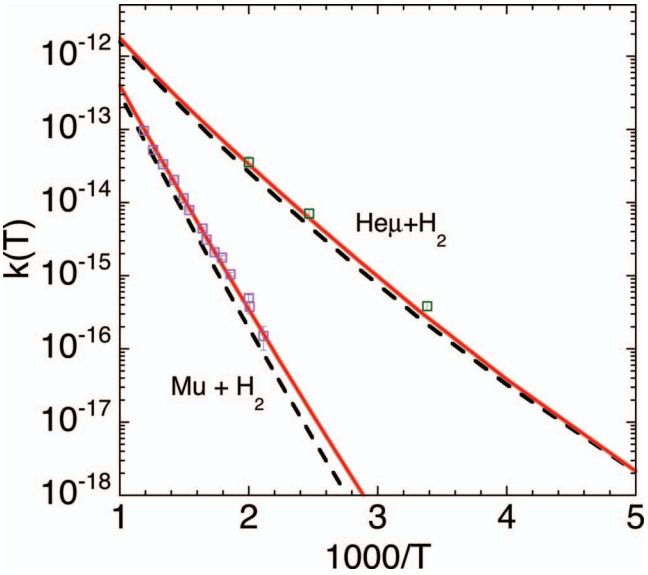

FIG. 9. Arrhenius plots of thermal rate constants for the Heμ + H_2 and Mu + H_2 reactions including accurate QM (solid red lines), ICVT/LAT (dashed black lines), the experimental data from Reid *et al.* for Mu + H_2,[9] and the new measurements for Heμ + H_2.

Very recently, Jambrina *et al.*[107] presented calculations for Mu + H_2 (and Heμ + H_2) using the BKMP2 (Ref. 101) BO PES together with an approximate adiabatic correction to the rate constant using Eq. (4) and a value of the barrier correction that was obtained using a value of the BODC at the saddle point. We note that when using this equation, one ideally should use a value of the barrier correction at the variational transition state; for Mu + H_2 the transition state is shifted strongly towards the products (R_{MuH} = 1.51 a_0, R_{HH} = 2.17 a_0) and the barrier correction at this location is 0.18 kcal/mol, which is significantly lower than the value of 0.37 kcal/mol used by Jambrina *et al.*[107] Their rate constants were only presented graphically, so precise comparisons to experiment or to our QM results are not possible.

Figure 9 compares the experimental measurements[9] for Mu + H_2 to accurate QM and ICVT/LAT results, with the Heμ + H_2 results plotted again for comparison. The marked difference in both magnitudes and slopes in comparing the Heμ + H_2 and Mu + H_2 results is noteworthy. Figure 10 compares experimental measurements for D + H_2 with the accurate QM and ICVT/LAT calculations on the BH PES. A similar comparison was made previously[41] for the BO PES together with the approximate barrier correction of Eq. (4) to account for the effect of the BODC, but the present results are expected to be more accurate.

Although the agreement between the QM calculations and the experimental measurements displayed in Figs. 8–10 seems quite impressive, the large ranges covered in these Arrhenius plots makes precise comparisons difficult. A more sensitive way to compare the data is to consider kinetic isotope effects. These are shown for $k_D/k_{He\mu}$ in Fig. 11(a) and

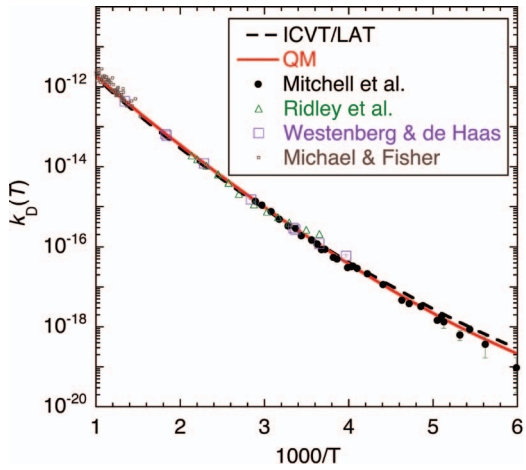

FIG. 10. Arrhenius plots of the QM thermal rate constants of the D + H_2 reaction on the BH surface compared with the ICVT/LAT calculations and with various experimental results.[37–40]

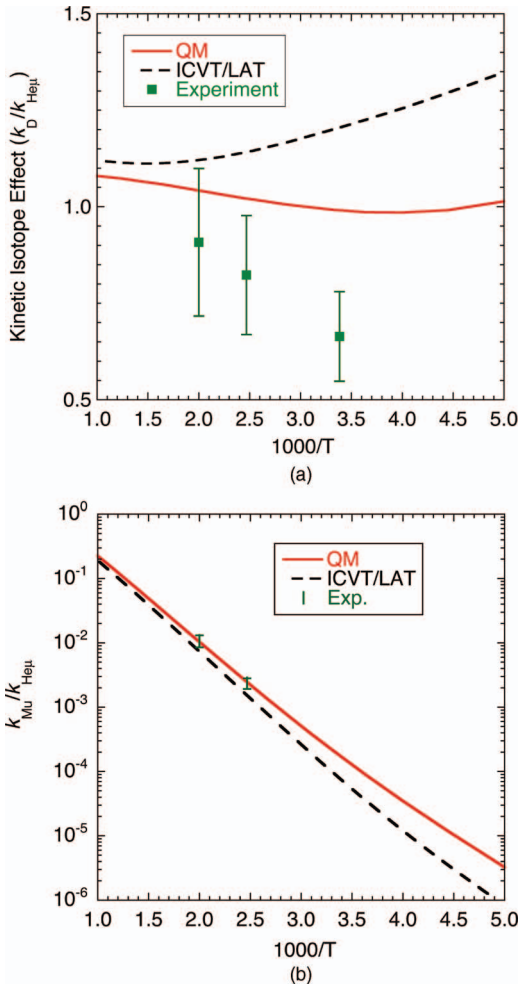

FIG. 11. Kinetic isotope effects. The experimental KIEs are obtained using fitted values for k_D and k_{Mu} with uncertainties estimated at 10% and using individual measurements for $k_{He\mu}$; (a) $k_D/k_{He\mu}$ and (b) $k_{Mu}/k_{He\mu}$. See Sec. IV.E in the text. The large error bars are the result of propagating independent errors in the ratio of rate constants. The experimental point at 405 K in (b) required extrapolation of k_{Mu} and this leads to additional uncertainty not reflected in the plotted error bar.

for $k_{Mu}/k_{He\mu}$ in Fig. 11(b). The plotted experimental KIEs used rate constants taken from the fits to the experimental data discussed above for k_D and k_{Mu} and individual measurements (taken from Table II) for $k_{He\mu}$. The uncertainty estimates are taken to be 10% for the fitted values. Although, individual k_D and k_{Mu} rate constant measurements have uncertainties that are in many cases significantly larger than this value, the fitting process is expected to reduce the statistical experimental uncertainties and the 10% value is an estimated upper bound; with this assumed value the uncertainties in the experimental KIEs are predominately due to the uncertainties in the individual $k_{He\mu}$ measurements.

As can be seen in Fig. 11(a), the accurate quantum $k_D/k_{He\mu}$ KIEs are close to unity at all temperatures. The uncertainty propagation for the experimental data leads to large error bars, and the experimental KIE at 500 K is in agreement with theory after accounting for these. The level of agreement for the 405 and 295.5 K points is poorer, although the trend to decreasing values with increasing temperature is present in both experiment and accurate quantum theory. VTST is encouragingly accurate for the rate constants (Table III and Fig. 8), being within ~30% of the QM calculations. This is a major success for variational transition state theory because the quantized vibrational energy of the forming MuH bond is very large,[10,11,108] and the ability of VTST with quantized partition functions to account for this rate constant is probably the most dramatic confirmation of the validity of the transition state procedure, dating back to Wigner and Eyring, of quantizing the partition functions of bound modes to turn the classically formulated theory into one capable of predicting rate constants for real molecules in a quantized world.

At a finer level of detail though, VTST does not reproduce the features in the KIEs in Fig. 11(a), and it exhibits the wrong trend with temperature down to about 250 K; this occurs because VTST is higher than accurate QM for k_D but lower than accurate QM for $k_{He\mu}$. The calculated QM Arrhenius activation energies for the two reactions are very similar with $E_a^{He\mu}$ having values of 6.51, 7.03, 7.33, and 8.80 kcal/mol at 295.5, 405, 500, and 1000 K, respectively, whereas E_a^D has values of 6.55, 7.11, 7.42, and 8.87 kcal/mol at 295.5, 405, 500, and 1000 K, respectively. The deviations between the activation energies and the BH saddle point energy of ~9.7 kcal/mol is mainly due to tunneling effects, especially at lower temperatures, and to zero point energy contributions.

The KIE comparisons between the QM results and experiment for $k_{Mu}/k_{He\mu}$ in Fig. 11(b) show better agreement than those for $k_D/k_{He\mu}$, and even the VTST results capture the correct qualitative trends. In part this is because of the large mass difference between Mu and Heμ that leads to a large change in the barrier location and the topography for the Mu–H_2 vibrationally adiabatic potential relative to that for other isotopes,[10,11,108] which results in a dramatic inverse KIE, whereas the much smaller mass difference between D and Heμ results in only a very subtle effect.

Although the mass of Heμ is twice that of D, the quantum mechanical rate constants for these two reactions differ by less than 10% over the entire temperature range studied. Even though the VTST results for the $k_D/k_{He\mu}$ KIEs differ quantitatively from the QM ones, they show this same

general feature of a KIE close to unity over the $T = 295.5$–500 K temperature range. Further insight into this feature in the KIEs can be understood by factoring the VTST results as described in Sec. IV.D.

The translational factor η_{trans} equals the ratio of the reduced masses from the translational partition functions raised to the 3/2 power, i.e., a factor of 1.556. The potential factor η_{pot} is different from unity if the variational transition states for the two reactions are not the same. Both reactions have the variational transition states shifted towards reactant, by about 0.15 and 0.12 a_0 for Heμ and D, respectively, and the small difference in the potential along the MEPs at these locations gives rise to a value for η_{pot} that increases from 0.78 to 0.86 for $T = 295.5$–500 K. (A factor less than one indicates that the potential for D is larger than that for Heμ.) The shift of the variational transition states towards reactants makes the stretch vibrations more reactant-like, leading to a value of the stretch vibration factor, η_{str}, that differs from unity by less than 1% for the same temperature range. The bend vibration has a lower frequency for the heavier isotope and a higher value for the bend partition function, leading to a value of η_{bend} that is also less than unity, increasing from 0.90 to 0.93 for $T = 295.5$–500 K. The rotational factor is due to the different moments of inertia at the variational transition states that leads to less energy being sequestered in overall rotation for Heμ + H_2 as compared to D + H_2. If we approximate the B constants using the moments of inertia at the collinear saddle point we get values of 5.49 and 7.04 cm^{-1} for Heμ + H_2 and D + H_2, respectively. The ratio of the values obtained with these B constant estimates is nearly constant for the experimental temperature range giving η_{rot} of 0.77. The final factor is from tunneling and nonclassical reflection; in the LAT approximation, this gives values that decrease from 1.43 to 1.16 over the $T = 295.5$–500 K temperature range. The only three factors that show any appreciable temperature dependence are the potential, bend vibrational, and tunneling/nonclassical reflection factors: η_{pot}, η_{bend}, and η_{tun}. The potential and bend vibrational factors increase with temperature, while the tunneling/nonclassical reflection factor decreases with temperature and they offset each other to give a product that varies only slightly, from 1.00 to 0.94 for $T = 295.5$–500 K. Including the other 3 nearly constant factors (η_{tran}, η_{str}, and η_{rot}) gives KIEs that decrease from 1.22 to 1.13. Over this same temperature range the QM KIEs vary from 0.99 to 1.04 (Table III).

The errors observed in the VTST calculations when compared to accurate QM calculations are likely to be predominantly due to a combination of approximations in the treatment of the tunneling and to uncertainties in the calculation of the threshold energies and effective potentials for tunneling due to the separable mode approximations as well as more-subtle dynamical effects that are discernable in the QM CRPs. The results can also be analyzed in terms of contributions from individual levels of the transition states as explained in detail in Refs. 68–72.

At the experimental temperatures, the Heμ + H_2 rate constants are most sensitive to the 0.5–0.8 eV total energy range that corresponds to flux that is gated by the first quantized transition state level, i.e., the [00^0] state, where the notation [v_1,$v_2{}^K$] specifies quantum numbers for the symmetric stretch (v_1), bend (v_2), and the vibrational angular momentum (K) (see Fig. 12). Thus, the temperature dependence of the $k_D/k_{He\mu}$ KIEs is largely due to the very small deviations in the threshold region. The Heμ + H_2 CRP for total angular momentum $J = 0$ [Fig. 12(a)] is systematically slightly higher than that for D + H_2 (and higher again than for H + H_2) showing a clear systematic mass dependence, but the ratio of the two differs most significantly in a small energy region near the threshold for the first transition state. The rate constants in the temperature range near $T = 200$–500 K are most sensitive to CRPs in this energy range, hence a relative minimum in the KIE is observed in that T range, as seen in Fig. 11(a). Figure 13 illustrates this effect further by plotting the Boltzmann weighting of the J-summed CRPs at the temperatures of the three experimental measurements of the Heμ + H_2 reaction to indicate the range of energies to which these rate constants are sensitive. As seen in the structure of the density of states, i.e., the energy derivative of the CRP, which is displayed in Fig. 12(b), the changes in the initial, [00^0],

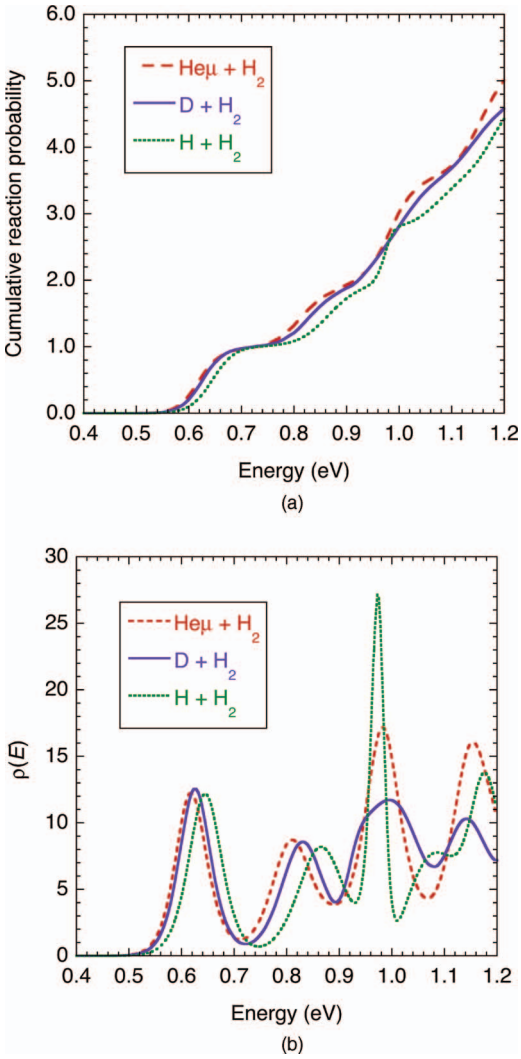

FIG. 12. (a) Cumulative reaction probabilities (CRPs) for 3 isotopes of H reacting with para H_2 for the case of $J = 0$ (the results for ortho H_2 are very similar). (b) Density of states (the energy derivative of the CRPs) corresponding to the results of panel (a).

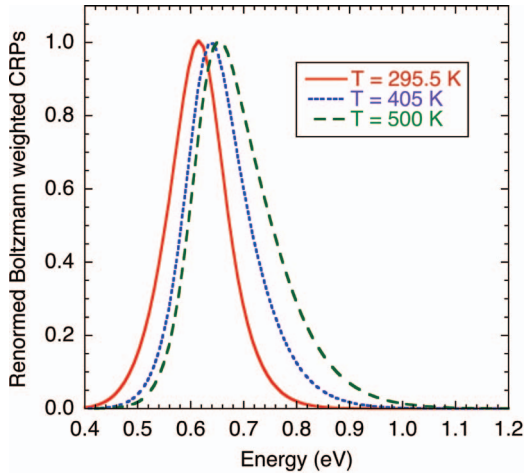

FIG. 13. Boltzmann weighted CRPs (summed over all J) for the Heμ + H_2 reaction renormalized so that their maximum value on the data grid is 1. These results indicate the energy ranges that contribute to the rate constants at the temperatures of the 3 measurements.

threshold energy and the subsequent spacing between transition state energies diminish when Heμ is substituted for D as compared to when D is substituted for H.

The kinetic isotope effects for $k_{Mu}/k_{He\mu}$ shown in Fig. 11(b) demonstrate excellent agreement between the experimental values and the accurate QM results. However, the experimental value at 405 K employs extrapolation to estimate the k_{Mu} rate constant and this introduces additional uncertainty. The ICVT/LAT results show the same trend with temperature as the accurate QM results, but the calculated KIE is 30% lower at 500 K and 74% lower at 200 K. Jambrina *et al.*[107] have recently reported a $k_{Mu}/k_{He\mu}$ KIE at 500 K of 0.0091 for QM calculations on the BKMP2 PES together with an approximate adiabatic correction. This is about 13% lower than the KIE we reported for the BH PES. As we mentioned earlier in this section, estimating the adiabatic correction for the Mu + H_2 rate constant at the variational transition state instead of at the classical barrier location (as Jambrina *et al.*[107] chose to do) would be expected to lead to better results. In particular, at 500 K using an adiabatic correction estimated at the transition state would have led to a value of k_{Mu} that is ~21% higher than what they reported, or a $k_{Mu}/k_{He\mu}$ KIE of about 0.011, which is about 6% higher than the value obtained on the accurate BH PES.

In marked contrast to the $k_D/k_{He\mu}$ KIEs, there is a large variation with temperature in the $k_{Mu}/k_{He\mu}$ KIEs, which is reflected in the large differences in activation energies found: $E_a^{Mu,QM}$ has values of 11.9, 13.0, 13.5, and 14.6 kcal/mol at 295.5, 405, 500, and 1000 K, respectively, whereas $E_a^{He\mu,QM}$ has values of 6.51, 7.03, 7.33, and 8.80 kcal/mol at these same temperatures. The much larger activation energy for the Mu + H_2 reaction is a consequence of the large ZPE shifts. Using the KIE analysis described above, the dominant contribution to the inverse isotope effect comes from the stretch vibration factor η_{str}, which varies from about 3 × 10^{-8} at 200 K to about 0.04 at 1000 K. This is primarily due to the *huge* change in ZPE associated with the factor of 36.1 change in isotopic mass from Heμ to Mu, which not only impacts the barrier height but also shifts the position of the variational TS well into the product valley.[7,10] This also has an important effect on the values for η_{pot} in the $k_{Mu}/k_{He\mu}$ KIE, which vary from 9.4 at 295.5 K to 3.7 at 500 K, in marked contrast to the range noted earlier for $k_D/k_{He\mu}$ of 0.78 to 0.86. The large change in the zero point vibrational energy associated with the formation of MuH was originally noted in early studies[9–11,108] of the Mu + H_2 and Mu + D_2 reactions.

VII. CONCLUDING REMARKS AND FUTURE STUDIES

The H + H_2 reaction has a long history as a prototype reaction in chemical kinetics, with early work[33] treating the H, D, and T isotopes. Later work added kinetic isotope effects for Mu.[9,108] Here we present the first detailed report, complementing recent communications,[31,32] of a reaction rate for the muonic helium atom, Heμ, with H_2. The present paper not only adds to the literature of the H + H_2 reaction, it also establishes the basis for the determination of rate constants for this heaviest H-atom by the μSR technique, and it allows comparison with the results of reaction rate theory on the accurate Born–Huang CCI potential energy surface. Although the experimental signal amplitudes are small, the measurements were successful, and the agreement with accurate quantum calculations is good to excellent at the two higher temperatures of the experiment, 405 and 500 K. At the lowest temperature of 295.5 K the level of agreement between quantum theory and experiment is less satisfactory, with the lower limit of the experiment, which also includes an estimated systematic error of 10%, being 22% higher than the QM result. However, further systematic error at 295.5 K, which was the most difficult point to obtain experimentally, cannot be ruled out.

Additional comparisons presented herein between accurate QM results on the BH surface and experiment for the rate constants of both the Mu + H_2 and D + H_2 reactions, over wide temperature ranges, confirm the generally excellent level of agreement found in similar comparisons for the Heμ + H_2 reaction, strongly supporting a claim[41] that the topic of thermal reaction rates on the H_3 system is effectively a "solved problem." There are very few examples in molecular quantum mechanics where a similar claim can be substantiated.

Any number of new experiments comparing the rates of Mu and Heμ reactivity suggest themselves, both on early barrier surfaces such as Mu + F_2 (Refs. 12 and 15) or Mu + N_2O,[21] where the demonstrated propensity for Mu tunneling would be dramatically offset by the much heavier Heμ atom mass, or on late-barrier surfaces such as Mu + CH_4, which is also an H-atom abstraction reaction like Mu + H_2,[19,20] and one that exhibits the highest activation energy yet measured in gas-phase Mu reactivity, about 1 eV.[109] The effect of the much heavier Heμ mass can again be expected to exhibit a huge increase in rate compared to the Mu-atom reaction due to dramatic changes in ZPE contributions at the transition state. Moreover, the CH_5 reaction system is an important starting point for the understanding of reaction rates on polyatomics, including recent studies of both ICVT/LAT (Refs. 19 and 20) and quantum calculations[110–112] of the Mu + CH_4 rate. A study of the Heμ + CH_4 reaction rate could provide a unique test of reaction rate theory

in the CH_5 system. Finally, it can be remarked that future studies comparing Mu and Heμ reactivity can be carried out on the same beam line and with the same apparatus, thereby reducing the level of systematic error that can often plague results of isotopic rate comparisons reported from different laboratories.

ACKNOWLEDGMENTS

We thank Dr. Syd Kreitzman for his management of the CMMS Facility and for the technical support it provides. A special thanks is given to Neil Aucoin for his engineering input and design of the heater for the target cell used in these experiments. We gratefully acknowledge NSERC for its financial support of this research. The work at Pacific Northwest National Laboratory (PNNL) was supported by the Chemical Sciences, Geosciences, and Biosciences Division of the Office of Basic Energy Science, U.S. Department of Energy (DOE). Battelle operates PNNL for DOE. The work at the University of Minnesota was supported in part by the DOE under Grant No. DE-FG02-86ER13579. The work at Northwestern was supported by AFOSR grant FA9550-10-1-0205.

[1] D. G. Fleming, Int. J. Radiat. Appl. Instrum. C Radiat. Phys. Chem. **28**, 115 (1986).
[2] M. Senba, D. G. Fleming, D. J. Arseneau, and H. R. Mayne, J. Chem. Phys. **112**, 9390 (2000).
[3] M. Senba, D. J. Arseneau, J. J. Pan, and D. G. Fleming, Phys. Rev. A **74**, 042708 (2006).
[4] D. G. Fleming and M. Senba, *Perspectives in Meson Science* (Kodansha, Tokyo, 1992).
[5] J. N. L. Connor, W. Jakubetz, and J. Manz, Chem. Phys. Lett. **45**, 265 (1977).
[6] D. K. Bondi, J. N. L. Connor, B. C. Garrett, and D. G. Truhlar, J. Chem. Phys. **78**, 5981 (1983).
[7] B. C. Garrett and D. G. Truhlar, J. Chem. Phys. **81**, 309 (1984).
[8] D. M. Garner, D. G. Fleming, and R. J. Mikula, Chem. Phys. Lett. **121**, 80 (1985).
[9] I. D. Reid, D. M. Garner, L. Y. Lee, M. Senba, D. J. Arseneau, and D. G. Fleming, J. Chem. Phys. **86**, 5578 (1987).
[10] B. C. Garrett, R. Steckler, and D. G. Truhlar, Hyperfine Interact. **32**, 779 (1986).
[11] R. Steckler, D. G. Truhlar, and B. C. Garrett, Int. J. Quantum Chem. Symp. **20**, 495 (1986).
[12] S. Baer, D. Fleming, D. Arseneau, M. Senba, and A. Gonzalez, in *Isotope Effects in Chemical Reactions and Photodissociation Processes*, ACS Symposium Series 502, edited by J. A. Kaye (American Chemical Society, Washington, DC, 1992), p. 111.
[13] G. C. Lynch, D. G. Truhlar, F. B. Brown, and J.-G. Zhao, J. Phys. Chem. **99**, 207 (1995).
[14] J. J. Pan, D. J. Arseneau, M. Senba, M. Shelly, and D. G. Fleming, J. Phys. Chem. A **101**, 8470 (1997).
[15] T. Takayanagi and Y. Kurosaki, J. Phys. Chem. A **101**, 7098 (1997).
[16] J. Villa, J. C. Corchado, A. Gonzalez-Lafont, J. M. Lluch, and D. G. Truhlar, J. Am. Chem. Soc. **120**, 12141 (1998).
[17] J. Villa, J. C. Corchado, A. Gonzalez-Lafont, J. M. Lluch, and D. G. Truhlar, J. Phys. Chem. A **103**, 5061 (1999).
[18] A. M. Lossack, E. Roduner, and D. M. Bartels, Phys. Chem. Chem. Phys. **3**, 2031 (2001).
[19] J. Pu and D. G. Truhlar, J. Chem. Phys. **117**, 10675 (2002).
[20] J. Pu and D. G. Truhlar, J. Chem. Phys. **116**, 1468 (2002).
[21] J. J. Pan, D. J. Arseneau, M. Senba, D. M. Garner, D. G. Fleming, T. Xie, and J. M. Bowman, J. Chem. Phys. **125**, 014307 (2006).
[22] T. Tanaka and T. Takayanagi, Chem. Phys. Lett. **496**, 248 (2010).
[23] Y. N. Kim, *Mesic Atoms and Nuclear Structure* (Elsevier, New York, 1971).
[24] V. S. Evseev and S. J. Amoretty, in *Muon Physics*, edited by V. Hughes and C. S. Wu (Academic Press, New York, 1975), Vol. III, p. 235.
[25] H. Orth, K. P. Arnold, P. O. Egan, M. Gladisch, W. Jacobs, J. Vetter, W. Wahl, M. Wigand, V. W. Hughes, and G. zu Putlitz, Phys. Rev. Lett. **45**, 1483 (1980).
[26] P. A. Souder, T. W. Crane, V. W. Hughes, D. C. Lu, H. Orth, H. W. Reist, M. H. Yam, and G. zu Putlitz, Phys. Rev. A **22**, 33 (1980).
[27] G. Audi, O. Bersillon, J. Blachot, and A. H. Wapstra, Nucl. Phys. A **729**, 3 (2003).
[28] C. J. Gardner, A. Badertscher, W. Beer, P. R. Bolton, P. O. Egan, M. Gladisch, M. Greene, V. W. Hughes, D. C. Lu, F. G. Mariam, P. A. Souder, H. Orth, J. Vetter, and G. zu Putlitz, Phys. Rev. Lett. **48**, 1168 (1982).
[29] A. S. Barton, P. Bogorad, G. D. Cates, H. Mabuchi, H. Middleton, N. R. Newbury, R. Holmes, J. McCracken, P. A. Souder, J. Xu, and D. Tupa, Phys. Rev. Lett. **70**, 758 (1993).
[30] F. G. Mariam, W. Beer, P. R. Bolton, P. O. Egan, C. J. Gardner, V. W. Hughes, D. C. Lu, P. A. Souder, H. Orth, J. Vetter, U. Moser, and G. zu Putlitz, Phys. Rev. Lett. **49**, 993 (1982).
[31] D. J. Arseneau, D. G. Fleming, O. Sukhorukov, J. H. Brewer, B. C. Garrett, and D. G. Truhlar, Physica B **404**, 946 (2009).
[32] D. G. Fleming, D. J. Arseneau, O. Sukhorukov, J. H. Brewer, S. L. Mielke, G. C. Schatz, B. C. Garrett, K. A. Peterson, and D. G. Truhlar, Science **331**, 448 (2011); We take this opportunity to correct some typographical errors in this communication: the mass of muonium is 0.114 amu, not 0.113 amu, the mass ratio of muonic helium to muonium is 36.1, not 36.4, and a positive muon is 206.77 times heavier than an electron rather than 206 times heavier.
[33] D. G. Truhlar and R. E. Wyatt, Annu. Rev. Phys. Chem. **27**, 1 (1976).
[34] H. Buchenau, J. P. Toennies, J. Arnold, and J. Wolfrum, Ber. Bunsenges. Phys. Chem. **94**, 1231 (1990).
[35] F. J. Aoiz, L. Banares, and V. J. Herrero, Int. Rev. Phys. Chem. **24**, 119 (2005).
[36] W. Hu and G. C. Schatz, J. Chem. Phys. **125**, 132301 (2006).
[37] B. A. Ridley, W. R. Schulz, and D. J. Le Roy, J. Chem. Phys. **44**, 3344 (1966).
[38] A. A. Westenberg and N. de Haas, J. Chem. Phys. **47**, 1393 (1967).
[39] D. N. Mitchell and D. J. Le Roy, J. Chem. Phys. **58**, 3449 (1973).
[40] J. V. Michael and J. R. Fisher, J. Phys. Chem. **94**, 3318 (1990).
[41] S. L. Mielke, K. A. Peterson, D. W. Schwenke, B. C. Garrett, D. G. Truhlar, J. V. Michael, M.-C. Su, and J. W. Sutherland, Phys. Rev. Lett. **91**, 063201 (2003).
[42] J. V. Michael, M.-C. Su, and J. W. Sutherland, J. Phys. Chem. A **108**, 432 (2004).
[43] E. Roduner, Appl. Magn. Reson. **13**, 1 (1997).
[44] C. Johnson, S. P. Cottrell, K. Ghandi, and D. G. Fleming, J. Phys. B **38**, 119 (2005).
[45] J. H. Brewer, A. M. Froese, B. A. Fryer, and K. Ghandi, Phys. Rev. A **72**, 022504 (2005).
[46] T. Suzuki, R. J. Mikula, D. M. Garner, D. G. Fleming, and D. F. Measday, Phys. Lett. B **95**, 202 (1980).
[47] D. J. Arseneau, D. M. Garner, M. Senba, and D. G. Fleming, J. Phys. Chem. **88**, 3688 (1984).
[48] R. J. Duchovic, A. F. Wagner, R. E. Turner, D. M. Garner, and D. G. Fleming, J. Chem. Phys. **94**, 2794 (1991).
[49] E. W. Lemmon, M. L. Huber, and J. W. Leachman, J. Res. Natl. Inst. Stand. Technol. **113**, 341 (2008).
[50] D. F. Measday, Phys. Rep. **354**, 243 (2001).
[51] F. James, MINUIT *Reference Manual* (CERN, Geneva, Switzerland, 1998).
[52] M. Senba, D. G. Fleming, D. J. Arseneau, D. M. Garner, and I. D. Reid, Phys. Rev. A **39**, 3871 (1989).
[53] M. Yang, J. Chem. Phys. **129**, 064315 (2008).
[54] T. Ko, P. Marshall, and A. Fontijn, J. Phys. Chem. **94**, 1401 (1990).
[55] C. J. Ballhausen and A. E. Hansen, Annu. Rev. Phys. Chem. **23**, 15 (1972).
[56] See supplementary material at http://dx.doi.org/10.1063/1.3657440 for additional QM calculations comparing to earlier approximate diagonal correction schemes for k_D, $k_D/k_{He\mu}$ KIE calculations on the BO CCI PES, and Mu + H_2 rate constants on the LSTH PES.
[57] S. L. Mielke, B. C. Garrett, and K. A. Peterson, J. Chem. Phys. **116**, 4142 (2002).
[58] S. L. Mielke, B. C. Garrett, and K. A. Peterson, J. Chem. Phys. **111**, 3806 (1999).
[59] S. L. Mielke, D. W. Schwenke, and K. A. Peterson, J. Chem. Phys. **122**, 224313 (2005).
[60] K. E. Riley and J. B. Anderson, J. Chem. Phys. **118**, 3437 (2003).
[61] M.-K. Chen and C.-S. Hsue, Phys. Rev. A **40**, 5520 (1989).

[62]S. L. Mielke, D. W. Schwenke, G. C. Schatz, B. C. Garrett, and K. A. Peterson, J. Phys. Chem. A **113**, 4479 (2009).
[63]Y. Sun, D. J. Kouri, and D. G. Truhlar, Nucl. Phys. A **508**, 41c (1990).
[64]Y. Sun, D. J. Kouri, D. G. Truhlar, and D. W. Schwenke, Phys. Rev. A **41**, 4857 (1990).
[65]D. W. Schwenke, S. L. Mielke, and D. G. Truhlar, Theor. Chim. Acta **79**, 241 (1991).
[66]W. H. Miller, J. Chem. Phys. **62**, 1899 (1975).
[67]S. L. Mielke, G. C. Lynch, D. G. Truhlar, and D. W. Schwenke, J. Phys. Chem. **98**, 8000 (1994).
[68]D. C. Chatfield, R. S. Friedman, D. G. Truhlar, B. C. Garrett, and D. G. Schwenke, J. Am. Chem. Soc. **113**, 486 (1991).
[69]D. C. Chatfield, R. S. Friedman, D. G. Truhlar, and D. W. Schwenke, Faraday Discuss. Chem. Soc. **91**, 289 (1991).
[70]D. C. Chatfield, R. S. Friedman, D. W. Schwenke, and D. G. Truhlar, J. Phys. Chem. **96**, 2414 (1992).
[71]D. C. Chatfield, R. S. Friedman, S. L. Mielke, D. W. Schwenke, G. C. Lynch, T. C. Allison, and D. G. Truhlar, in *Dynamics of Molecules and Chemical Reactions*, edited by R. E. Wyatt and J. Z. H. Zhang (Marcel Dekker, New York, 1996), p. 323.
[72]D. C. Chatfield, S. L. Mielke, T. C. Allison, and D. G. Truhlar, J. Chem. Phys. **112**, 8387 (2000).
[73]H. Eyring, J. Chem. Phys. **3**, 107 (1935).
[74]E. B. Wilson, Jr., J. C. Decius, and P. C. Cross, *Molecular Vibrations* (McGraw-Hill, New York, 1955).
[75]K. Takayanagi, Prog. Theor. Phys. **8**, 497 (1952).
[76]M. C. Colton and G. C. Schatz, Intern. J. Chem. Kinet. **18**, 961 (1986).
[77]J. M. Bowman, Adv. Chem. Phys. **61**, 115 (1985).
[78]S. L. Mielke, G. C. Lynch, D. G. Truhlar, and D. W. Schwenke, Chem. Phys. Lett. **216**, 441 (1993).
[79]G. C. Schatz, D. Sokolovski, and J. N. L. Connor, J. Chem. Phys. **94**, 4311 (1991).
[80]J. M. Bowman, Theor. Chem. Acc. **108**, 125 (2002).
[81]D. G. Truhlar and B. C. Garrett, in *Annual Review of Physical Chemistry*, edited by B. S. Rabinovitch, J. M. Schurr, and H. L. Strauss (Annual Reviews, Inc., Palo Alto, CA, 1984), vol. 35, p. 159.
[82]B. C. Garrett and D. G. Truhlar, J. Chem. Phys. **72**, 3460 (1980).
[83]B. C. Garrett, D. G. Truhlar, R. S. Grev, and A. W. Magnuson, J. Phys. Chem. **84**, 1730 (1980); B. C. Garrett, D. G. Truhlar, R. S. Grev, and A. W. Magnuson, J. Phys. Chem. **87**, 4554(E) (1983).
[84]B. C. Garrett and D. G. Truhlar, J. Chem. Phys. **79**, 4931 (1983).
[85]Y.-P. Liu, D.-h. Lu, A. Gonzalez-Lafont, D. G. Truhlar, and B. C. Garrett, J. Am. Chem. Soc. **115**, 7806 (1993).
[86]B. C. Garrett and D. G. Truhlar, J. Phys. Chem. **95**, 10374 (1991).
[87]B. C. Garrett, G. C. Lynch, T. C. Allison, and D. G. Truhlar, Comput. Phys. Commun. **109**, 47 (1998).
[88]D. G. Truhlar and B. C. Garrett, Acc. Chem. Res. **13**, 440 (1980).
[89]D. G. Truhlar, A. D. Isaacson, R. T. Skodje, and B. C. Garrett, J. Phys. Chem. **86**, 2252 (1982); **87**, 4554(E) (1983).
[90]B. C. Garrett and D. G. Truhlar, J. Phys. Chem. **83**, 1079 (1979); **84**, 682(E) (1980); **87**, 4554(E) (1983).
[91]G. A. Natanson, J. Chem. Phys. **93**, 6589 (1990).
[92]S. C. Tucker, D. G. Truhlar, B. C. Garrett, and A. D. Isaacson, J. Chem. Phys. **82**, 4102 (1985).
[93]D. G. Truhlar, D.-h. Lu, S. C. Tucker, X. G. Zhao, A. Gonzalez-Lafont, T. N. Truong, D. Maurice, Y.-P. Liu, and G. C. Lynch, in *Isotope Effects in Chemical Reactions and Photodissociation Processes*, ACS Symposium Series 502, edited by J. A. Kaye (American Chemical Society, Washington, DC, 1992), p. 16.
[94]J. Zheng and D. G. Truhlar, Phys. Chem. Chem. Phys. **12**, 7782 (2010).
[95]W. R. Schulz and D. J. Le Roy, Can. J. Chem. **42**, 2480 (1965).
[96]J. V. Michael, J. Chem. Phys. **92**, 3394 (1990).
[97]I. S. Jayaweera and P. D. Pacey, J. Phys. Chem. **94**, 3614 (1990).
[98]L. Banares and M. J. D'Mello, Chem. Phys. Lett. **277**, 465 (1997).
[99]D. G. Truhlar and C. J. Horowitz, J. Chem. Phys. **68**, 2466 (1978).
[100]A. I. Boothroyd, W. J. Keogh, P. G. Martin, and M. R. Peterson, J. Chem. Phys. **95**, 4343 (1991).
[101]A. I. Boothroyd, W. J. Keogh, P. G. Martin, and M. R. Peterson, J. Chem. Phys. **104**, 7139 (1996).
[102]G. C. Schatz, J. Chem. Phys. **83**, 3441 (1985).
[103]K. Tsuda, K. Moribayashi, and H. Nakamura, J. Chem. Phys. **103**, 5512 (1995).
[104]K. Tsuda, K. Moribayashi, and H. Nakamura, Chem. Phys. Lett. **231**, 439 (1994).
[105]B. Liu, J. Chem. Phys. **58**, 1925 (1973).
[106]P. Siegbahn and B. Liu, J. Chem. Phys. **68**, 2457 (1978).
[107]P. G. Jambrina, E. García, V. J. Herrero, V. Sáez-Rábanos, and F. J. Aoiz, J. Chem. Phys. **135**, 034310 (2011).
[108]D. K. Bondi, D. C. Clary, J. N. L. Connor, B. C. Garrett, and D. G. Truhlar, J. Chem. Phys. **76**, 4986 (1982).
[109]R. Snooks, D. J. Arseneau, D. G. Fleming, M. Senba, J. J. Pan, M. Shelley, and S. Baer, J. Chem. Phys. **102**, 4860 (1995).
[110]B. Kerkeni and D. C. Clary, Chem. Phys. Lett. **421**, 499 (2006).
[111]B. Kerkeni and D. C. Clary, J. Chem. Phys. **120**, 2308 (2004).
[112]S. T. Banks and D. C. Clary, J. Chem. Phys. **130**, 024106 (2009).